Robust Evidence C-Means Clustering Combining Spatial Information for Image Segmentation

Rong Lan
  Xi'an University of Posts and Telecommunications

Haowen Mi (✉ 1466403072@qq.com)
  Xi'an University of Posts and Telecommunications

Na Qu
  Xi'an University of Posts and Telecommunications

Feng Zhao
  Xi'an University of Posts and Telecommunications

Haiyan Yu
  Xi'an University of Posts and Telecommunications

Lu Zhang
  Xi'an University of Posts and Telecommunications

Research Article

Additional Declarations: No competing interests reported.

Robust Evidence C-Means Clustering Combining Spatial Information for Image Segmentation

Rong Lan[1] · Haowen Mi[1] · Na Qu[1] · Feng Zhao[1] · Haiyan Yu[1] · Lu Zhang[1]

Abstract Although evidence c-means clustering (ECM) based on evidence theory overcomes the limitations of fuzzy theory to some extent and improves the capability of fuzzy c-means clustering (FCM) to express and process the uncertainty of information, the ECM does not consider the spatial information of pixels, which makes it to be unable to effectively deal with noise pixels. Applying ECM directly to image segmentation cannot obtain satisfactory results. This paper proposes a robust evidence c-means clustering combining spatial information for image segmentation algorithm. Firstly, an adaptive noise distance is constructed by using the local information of pixels to improve the ability to detect noise points. Secondly, the pixel's original, local and non-local information are introduced into the objective function through adaptive weights to enhance the robustness to noise. Then, the entropy of pixel membership degree is used to design an adaptive parameter to solve the problem of distance parameter selection in credal c-means clustering (CCM). Finally, the Dempster's rule of combination was improved by introducing spatial neighborhood information, which is used to assign the pixels belonging to the meta-cluster and the noise cluster into the singleton cluster. Experiments on synthetic images, real images and remote sensing SAR images demonstrate that the proposed algorithm not only suppress noise effectively, but also retain the details of the image. Both the segmentation visual effect and evaluation indexes indicate its effectiveness in image segmentation.

1 Introduction

As an important pre-processing step of image analysis, image understanding and image description, image segmentation aims to assign pixels to several categories enabling pixels belonging to the same category have strong correlation. Heretofore, many image segmentation methods have been proposed to address the image segmentation problems in different situations [1]. The commonly used image segmentation methods include threshold-based algorithm, edge-based algorithm, region-based algorithm, graph-based algorithm and clustering-based algorithm [2-6]. Clustering analysis as an unsupervised learning method is an important tool in data mining [7]. Presently various clustering algorithms have been proposed. Since there is no need to label the image pixels, clustering algorithm are commonly used in image segmentation [8]. As a clustering algorithm based on fuzzy theory, FCM is widely applied in image segmentation for its simplicity. However, fuzzy theory has certain limitations [9], thus limiting the capability of FCM to describe uncertainty of information, resulting in its inability to effectively handle boundary pixels. Simultaneously, the FCM algorithm is more sensitive to noise or outliers since the neighborhood information of pixels is not considered.

In view of the above disadvantages of FCM, Dave [10] proposed a noise clustering (NC), which introduces the concept of noise cluster on the basis of FCM. The outliers are assigned to the noise cluster by noise distance, which re-

✉ Rong Lan
ronglanlogic@163.com

Haowen Mi
1466403072@qq.com

[1] School of Telecommunication and Information Engineering, Xi'an University of Posts and Telecommunications, Xi'an, People's Republic of China

duces the influence of outliers on the clustering result to some extent. Ahmed et al [11] proposed a fuzzy c-means clustering with spatial information constraint (FCM_S), which enhances the robustness of FCM. Due to the high time cost of computing spatial information, Chen and Zhang [12] proposed FCM_S1 and FCM_S2, which improves the efficiency of FCM_S by replacing the spatial information with the neighborhood mean or median value. For noisy images, the effectiveness of local information may decrease with the increase of noise intensity. Thus, Zhao et al [13] proposed a fuzzy c-means clustering with non-local spatial information (FCM_NLS), which further improves the anti-noise performance of the algorithm. In the above algorithms, the parameter that controls the local or non-local spatial information constraint needs to be manually selected. To solve the parameter selection problem, Krinidis et al [14] proposed a robust fuzzy local information c-means clustering (FLICM). The FLICM algorithm introduces the local spatial information and local gray information of pixels into the objective function in the form of a local fuzzy factor, which preserves rich detail information while resisting noise. Lei et al [15] proposed a fast and robust fuzzy c-means clustering (FR-FCM) based on morphological reconstruction and membership filtering. The FRFCM algorithm is faster and more robust than FCM, but it cannot effectively handle weak edge regions contaminated by noise. Wang et al [16] proposed a robust fuzzy c-means clustering with adaptive spatial and intensity constraint and membership linking (FCM_SICM). The FCM_SICM algorithm first acquires the local spatial and intensity information by fast bilateral filtering before clustering. Then, the spatial intensity information is introduced into the objective function through adaptive weight. Finally, the number of iterations is reduced through membership linking. In order to further improve the robustness of FLICM, Zhang et al [17] introduced non-local information into FLICM and proposed a FLICM with local and non-local information (FLICMLNLI). The FLICMLNLI algorithm utilizes the two distances from a pixel and its neighborhood pixels to the cluster center. However, assigning the same weight to these two different distances may incorrectly magnify the importance of the neighborhood information. Therefore, Song et al [18] proposed a self-learning weighted fuzzy local information clustering integrating local and non-local information. This algorithm calculates distance weights by self-learning and adaptively balances the anti-noise ability and detail retention ability.

In order to extend the existing hard, fuzzy and possibilistic partition and improve the processing ability of FCM for uncertain and imprecise data. Masson et al [19] integrated and improved FCM and NC, proposed an evidence c-means clustering (ECM) based on the concept of credal partition under the theoretical framework of belief functions. For objects that cannot be precisely assigned, ECM assigns them to meta-clusters united by several singleton clusters, which reduces the risk of misclassification. Meanwhile, the inclusion of the noise cluster makes the ECM algorithm overcome the influence of outliers to a certain extent. In ECM, when the center of a meta-cluster is close to the center of a singleton cluster, it may produce unreasonable clustering results. Therefore, Liu et al [20] proposed a belief c-means clustering (BCM). In BCM, the mass of belief on a meta-cluster is calculated according to the distance between the object and the centers of singleton clusters (contained in the meta-cluster) and the distance between the centers of these singleton clusters, so it is not necessary to calculate the center of the meta-cluster. Due to the complexity of using and implementing BCM, Liu et al [21] proposed a credal c-means clustering (CCM) to overcome the limitations of ECM. In CCM, an object has a higher probability of being assigned to the meta-cluster if it is close to both a meta-cluster and singleton clusters contained in the meta-cluster. To address the problem that the ECM needs to determine the number of clusters in advance, Su et al [22] proposed an evolutionary version of evidential c-means clustering (E2CM). E2CM is based on a variable string length artificial bee colony (VABC) algorithm, which can optimize the number of clusters and the center position at the same time. Although credal partition has outstanding advantage in depicting uncertainty and imprecision, it is time-consuming due to a lot of redundant computations. To overcome the drawbacks of high time complexity and long running time of ECM and CCM, Zhang et al [23] proposed a dynamic evidential clustering (DEC), which includes two steps: preliminary adaptive credal partition and partial credal redistribution. In the preliminary adaptive credal partition, by minimizing an objective function similar to FCM, the mass of beliefs of each object belonging to the single cluster and the noise cluster is obtained. Then a given rule is used to adaptively assign all objects as outliers, precise points or imprecise points. For imprecise points, the mass of beliefs on each cluster is reassigned by partial credal redistribution with the corresponding dynamic frame of discernment. In the field of image segmentation, Zhu [24] proposed an algorithm for image segmentation using automatic determined mass functions. This algorithm uses the membership degrees of the center pixel and neighborhood pixels to determine the mass function of the center pixel, then uses Dempster's rule of combination and decision to achieve image segmentation. Wen et al [25] proposed an improved evidential fuzzy c-means algorithm for MRI image segmentation. This algorithm first fuses the input image averagely to reduce the uncertainty and conflicting information in the image. Then one mass function is generated using the membership degree of the center pixel and the other mass function is generated using the membership degrees and spatial information of neighborhood pixels. Finally, evidence theory is used to implement image segmenta-

tion and sensor data fusion. Makni et al [26] introduced local information into ECM and took the spatial distance as the weight to combine the mass functions of the center pixel and neighborhood pixels by using Dempster's rule of combination, and applied this algorithm to prostate multi-parametric MRI image segmentation. Wang et al [27] proposed an adaptive kernelized evidential clustering (AKEC), which uses adaptive kernel distance instead of Euclidean distance and introduces local information into the objective function to achieve automatic 3D tumor segmentation in FDG–PET images.

In conclusion, ECM improves the capability of traditional FCM to deal with boundary points and outliers. However, ECM does not introduce any spatial information, resulting in it cannot segment noisy images effectively. To further improve the robustness of ECM, this paper proposes a robust evidence c-means clustering combining spatial information for image segmentation algorithm. The main contributions of the proposed algorithm are summarized as follows:

(1) In order to avoid the influence of the noise distance proposed for general dataset on the performance of the image segmentation algorithm, an adaptive noise distance is constructed by using the probability that the pixel is a noise point. This proposed adaptive noise distance is used to assign the detected noise points to the noise cluster, thus reducing the impact of noise points on image segmentation.

(2) To effectively deal with high intensity noise in the local window, local and non-local information of pixels are introduced in the objective function of ECM. A parameter for evaluating the reliability of the local window is defined and the weights of the original ECM term and the spatial information term are adaptively determined by combining the noise probability.

(3) The distance metric between pixel and the meta-cluster in CCM is improved. The entropy of pixel membership degree is used to define an adaptive parameter, which solves the problem that the distance parameter in CCM need to be selected manually.

(4) To obtain the final segmentation image, the Dempster's rule of combination was improved by introducing spatial neighborhood information, which is used to assign the pixels belonging to the meta-cluster and the noise cluster into the singleton cluster.

The rest of this paper is organized as follows. Section 2 introduces the work related to the proposed algorithm. Section 3 describes the proposed algorithm in detail. Section 4 is the comparison experiments and results analysis. Section 5 draws the conclusion.

2 Related work

2.1 Belief functions

Dempster-Shafer evidence theory, as a generalization of probability theory, is a mathematical method to deal with uncertain reasoning problems [28].

Let $\Omega = \{\omega_1, \cdots, \omega_c\}$ be a set of clusters to which object x belongs and the finite elements in Ω are mutually exclusive, then Ω is called the frame of discernment of object x. The set consists of all subsets of Ω is called the power-set of Ω, denoted by 2^{Ω}.

The basic belief assignment (BBA) is denoted as $m(\cdot)$, also known as the mass of belief, satisfying $\sum_{A \subseteq \Omega} m(A) = 1$, $0 \le m(A) \le 1$. The BBA maps the membership degree of object x belonging to a subset of Ω to $[0, 1]$. Let the dataset $X = \{x_1, \cdots, x_n\}$, the BBA of x_i is denoted as m_i, then $M = \{m_1, \cdots, m_n\}$ is defined as a credal partition of dataset X.

The BBA can be transformed into the pignistic probability by pignistic transformation [29], then the object can be assigned to a specific singleton cluster according to the pignistic probability. The pignistic probability is calculated as:

$$BetP(\omega) = \sum_{A \subseteq \Omega, A \neq \varnothing, \omega \in A} \frac{1}{|A|} \frac{m(A)}{1 - m(\varnothing)} \tag{1}$$

where $|A|$ denotes the cardinality of the non-empty subset A. The fuzzy partition of data set X is obtained by transforming $m(\cdot)$ to $BetP(\cdot)$ for each object, where $BetP_i(\omega_j)$ represents the membership degree of x_i belonging to ω_j.

Let m_1 and m_2 represent two independent BPAs on the frame of discernment Ω. The combined BBA is obtained by Dempster's rule of combination [28]:

$$(m_1 \oplus m_2)(A) = \begin{cases} \frac{\sum_{B \cap C = A} m_1(B)m_2(C)}{1-K}, & A \neq \emptyset, A, B, C \subseteq \Omega \\ 0, & A = \emptyset \end{cases} \tag{2}$$

where $K = \sum_{B \cap C = \emptyset} m_1(B) m_2(C)$ denotes the degree of conflict between m_1 and m_2.

2.2 Evidence c-means clustering algorithm

ECM is a clustering algorithm based on the concept of credal partition. In ECM, the object can be assigned not only to the noise cluster or singleton cluster, but also to the meta-cluster united by several singleton clusters. Extending the existing c clusters into 2^c clusters is a significant feature of ECM. This additional flexibility is beneficial to describe the uncertainty of the dataset more accurately and improve the robustness to outliers.

Let $X = \{x_1, \cdots, x_n\}$ be the objects to be assigned and $\Omega = \{\omega_1, \cdots, \omega_c\}$ be the frame of discernment of X. The objective function is defined as follows:

$$J_{ECM} = \sum_{i=1}^{n} \sum_{\{j|A_j \subseteq \Omega, A_j \neq \emptyset\}} c_j^{\alpha} m_{ij}^{\beta} d_{ij}^2 + \sum_{i=1}^{n} \delta^2 m_{i\emptyset}^{\beta} \tag{3}$$

where $c_j = |A_j|$ denotes the cardinality of the non-empty subset A_j. The weighting coefficient c_j^{α} aims at penalizing the subset A_j with high cardinality, α is used to control the degree of penalization. $m_{ij} = m_i(A_j)$ and $m_{i\emptyset} = m_i(\emptyset)$ represent the mass of belief of object x_i belonging to cluster A_j and the noise cluster respectively. β is used to control the fuzziness of the partition. δ denotes the distance between the object and the noise cluster, which is calculated as follows:

$$\delta = \sqrt{\frac{\lambda}{c \cdot n} \left(\sum_{i=1}^{n} \sum_{j=1}^{c} dis_{ij}^2 \right)} \tag{4}$$

where dis_{ij} denotes the distance between object x_i and the j th cluster center obtained by FCM. λ is a parameter that needs to be manually selected.

In Eq. (3), d_{ij} denotes the distance between object x_i and cluster A_j, which is calculated as follows:

$$d_{ij} = \left\| x_i - \overline{v_j} \right\| \tag{5}$$

$$\overline{v_j} = \frac{1}{c_j} \sum_{k=1}^{c} s_{kj} v_k \tag{6}$$

$$s_{kj} = \begin{cases} 1, & \omega_k \in A_j \\ 0, & \omega_k \notin A_j \end{cases} \tag{7}$$

where v_k denotes the center of singleton cluster ω_k and $\overline{v_j}$ denotes the barycenter of meta-cluster A_j.

Utilizing the Lagrange multiplier method, the update formulas of m_{ij} and $m_{i\emptyset}$ can be obtained by:

$$m_{ij} = \frac{c_j^{-\alpha/(\beta-1)} d_{ij}^{-2/(\beta-1)}}{\sum_{A_k \neq \emptyset} c_k^{-\alpha/(\beta-1)} d_{ik}^{-2/(\beta-1)} + \delta^{-2/(\beta-1)}} \tag{8}$$

$$m_{i\emptyset} = 1 - \sum_{A_j \neq \emptyset} m_{ij} \tag{9}$$

The cluster center matrix V is the solution of the following linear equations:

$$HV = B \tag{10}$$

where H is a matrix of size $c \times c$, V is a matrix of size $c \times p$, B is a matrix of size $c \times p$. c is the number of clusters, p is the dimension of objects and cluster centers.

The elements in matrix H are calculated as follows:

$$H_{lk} = \sum_{i=1}^{n} \sum_{A_j \neq \emptyset} c_j^{\alpha-2} m_{ij}^{\beta} s_{lj} s_{kj} = \sum_{i=1}^{n} \sum_{\{\omega_l, \omega_k\} \subseteq A_j} c_j^{\alpha-2} m_{ij}^{\beta} \tag{11}$$
$$l, k = 1, \cdots, c$$

The elements in matrix B are calculated as follows:

$$B_{lq} = \sum_{i=1}^{n} x_{iq} \sum_{A_j \neq \emptyset} c_j^{\alpha-1} m_{ij}^{\beta} s_{lj} = \sum_{i=1}^{n} x_{iq} \sum_{\omega_l \in A_j} c_j^{\alpha-1} m_{ij}^{\beta} \tag{12}$$
$$l = 1, \cdots, c, q = 1, \cdots p$$

3 The proposed algorithm

Applying ECM directly to image segmentation has the following problems: First, the noise cluster in ECM directly refers to the definition in NC [10]. For noisy images, the selection of parameter λ in the original definition of noise distance will affect the capability of the algorithm to detect noise points. Second, ECM is proposed for general dataset without considering the spatial information of pixels, which makes it impossible to effectively segment noisy images. Third, it lacks a strategy for assigning pixels belonging to the meta-cluster and the noise cluster to a specific singleton cluster. Aiming at the above problems of ECM, this paper proposes a robust evidence c-means clustering combining spatial information for image segmentation algorithm. The proposed algorithm mainly includes three steps: deriving a credal partition, specifying meta-clusters, recovering the noise cluster. The framework is shown in Fig. 1.

First, an adaptive noise distance is constructed to improve the algorithm's capability to detect noise points. Then, the spatial information of pixels is adaptively introduced to calculate the distance between the pixel and the cluster center, while a distance parameter in CCM is determined adaptively. After iteration termination, the credal partition is derived. Finally, through Dempster's rule of combination introducing spatial neighborhood information, the meta-clusters are first specified and then the noise cluster is recovered to obtain the segmentation image.

3.1 Deriving a credal partition

Deriving a credal partition is the first step of the proposed algorithm. The main purpose of this step is to obtain the mass of belief on each cluster for any pixel and then determine the classification of pixels based on the mass of belief. It is primarily necessary to determine the kinds of cluster in the proposed algorithm.

In an image, it is difficult to determine the classification of pixels located in the boundary region. These pixels may be assigned similar membership degrees to singleton clusters that are close to them, i.e., the gray values of these pixels are closer to the barycenter of a meta-cluster composed of two close singleton clusters. From the perspective of credal partition, it is more reasonable to assign these pixels with high uncertainty to a meta-cluster. Since the boundary region of an image is often between two singleton clusters, there is no need to consider a meta-cluster composed of
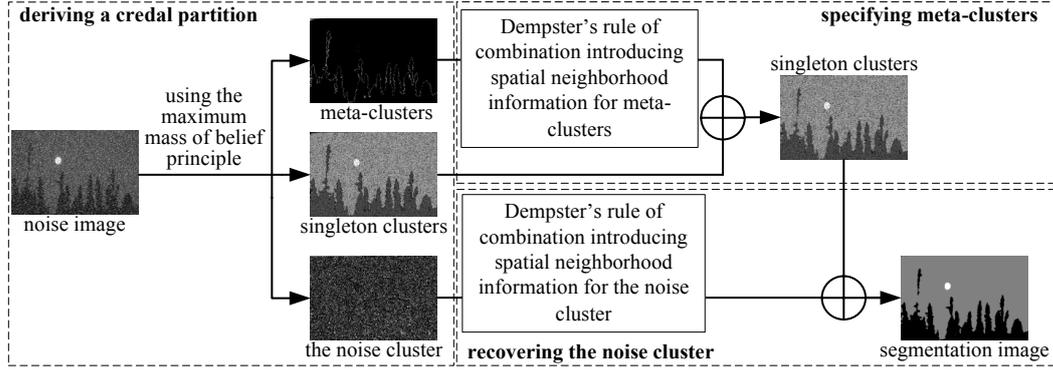
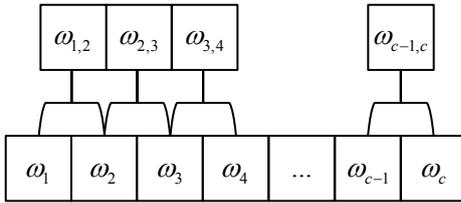**Fig. 1** The framework of the proposed algorithm

Fig. 2 Composition of meta-clusters

more than two singleton clusters. Based on the above analysis, three kinds of clusters are determined, which are the noise cluster, singleton clusters and meta-clusters. As shown in Fig. 2, the meta-cluster is composed of two adjacent singleton clusters. After obtaining the centers $V = \{v_1, \cdots, v_c\}$ of c singleton clusters, the barycenter of $c-1$ meta-clusters are calculated by Eq. (6) and Eq. (7).

When determining the classification of pixels, constructing reasonable distance measurement formulas is conducive to improving the accuracy of discrimination. Therefore, after determining the kinds of clusters, defining the distance measurement formulas between the pixel and the three kinds of clusters according to the characteristics of the different clusters is the key problem to be solved in this section. Finally, the defined distance measurement formulas are substituted into the objective function and the credal partition of pixels is obtained by minimizing the objective function. The specific steps are as follows.

3.1.1 Distance metric between the pixel and the noise cluster

The distance between pixels and the noise cluster is called the noise distance, which affects the detection of noise pixels. In an image, the pixels that are heavily contaminated by noise need to be assigned to the noise cluster using a smaller noise distance. On the contrary, they should be far away from the noise cluster. In ECM, the noise distance obtained by Eq. (4) cannot be calculated adaptively according to the degree of noise contamination of pixels. Also, for different images, it is necessary to select the best value of parameter λ by experiment. If the value of λ is too large, the noise pixels will not be assigned to the noise cluster.

In this paper, the degree to which a pixel is affected by noise is characterized as the probability that the pixel being a noise point i.e., the higher the probability that a pixel is a noise pixel, the more seriously the original gray information of the pixel is corrupted by noise. Intuitively, the higher the noise probability, the smaller the noise distance should be. Therefore, the noise distance δ_i between pixel x_i and the noise cluster can be defined as:

$$\delta_i = \frac{1 - p_{i\emptyset}}{p_{i\emptyset} + eps} d_i^{\min} \tag{13}$$

where eps is a small positive number to avoid the denominator equaling to 0, $p_{i\emptyset}$ denotes the probability that pixel x_i is a noise pixel and $d_i^{\min}$ denotes the minimum distance between pixel x_i and cluster centers.

In Eq. (13), δ_i is close to positive infinity when $p_{i\emptyset} = 0$, δ_i equals $d_i^{\min}$ when $p_{i\emptyset} = 0.5$ and δ_i is 0 when $p_{i\emptyset} = 1$. It can be found that the higher the probability that pixel x_i is a noise pixel, the smaller the distance between pixel x_i and the noise cluster.

In order to calculate the noise probability $p_{i\emptyset}$, the neighborhood pixels of pixel x_i need to be fully utilized. First, the reliable neighborhood pixels that are weakly contaminated by noise are found. Then, the similarity of the gray value between center pixel x_i and neighborhood pixels is measured. When the center pixel x_i is more similar to neighborhood pixels with high reliability, the noise probability of pixel x_i is smaller. Therefore, by defining the calculation formula for evaluating the similarity and reliability of pixel gray value, $p_{i\emptyset}$ is defined as follows:

$$p_{i\emptyset} = 1 - \frac{\sum\limits_{r \in N_i} w_r s_{ir}}{\sum\limits_{r \in N_i} s_{ir}} \tag{14}$$

where N_i denotes a local window centered at pixel x_i, s_{ir} denotes the similarity between pixel x_i and pixel x_r, w_r denotes the reliability of pixel x_r.
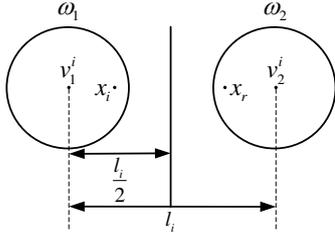
Fig. 3 Clustering result of FCM for pixel x_i and pixel x_r, pixel x_i belongs to cluster ω_1 and pixel x_r belongs to cluster ω_2

Higher reliability means that pixel x_r is less corrupted by noise and the gray value is closer to the original value. In Eq. (14), if there are many pixels with high reliability in local window N_i and pixel x_i has a similar gray value to these pixels, then $p_{i\emptyset}$ is small.

Before defining the reliability of a pixel, the formula for measuring the similarity between the center pixel x_i and the neighborhood pixel x_r is first defined. In general, the closer the gray value between two pixels, the higher the similarity. However, in the noisy image, if the centers of two singleton clusters are not far apart, the gray value of pixels belonging to one of the clusters may be shifted toward the other cluster due to the presence of noise, resulting in two pixels belonging to different singleton clusters having high similarity. Therefore, the distance between centers of adjacent singleton clusters is fully considered when calculating the similarity s_{ir}. Thus, s_{ir} is defined as follows:

$$s_{ir} = e^{-\frac{\|x_i - x_r\|^2}{G_i}} \tag{15}$$

where the value of G_i depends on the distance between the singleton cluster centers.

For an image, the clustering result of pixels is obtained by FCM algorithm in advance. As shown in Fig. 3, let the two adjacent singleton clusters nearest to x_i be ω_1 and ω_2, with centers v_1^i and v_2^i, respectively, and let $l_i = \|v_1^i - v_2^i\|$. Then, G_i is calculated as follows:

$$G_i = \left[1 - \log_2\left(1 + \sqrt{\frac{l_i}{255}}\right)\right] \left(\frac{l_i}{2}\right)^2 \tag{16}$$

Combining Fig. 3 with Eq. (16), it can be seen that the closer the centers of two adjacent singleton clusters are, the smaller l_i is and the smaller G_i is, resulting in the similarity s_{ir} decay faster and preventing a higher similarity between pixel x_i belonging to ω_1 and pixel x_r belonging to ω_2. On the contrary, as l_i increases, G_i is not too large, preventing the similarity s_{ir} from decaying too slowly.

In order to calculate the reliability of pixels in the local window N_i, a reliable gray value needs to be determined as a reference value. Morphological reconstruction is able to preserve the contour of the object in the image and remove the noise without prior knowledge of the type of noise

[30]. Therefore, in this paper, the noisy image is filtered using morphological closing reconstruction proposed in [15], which is defined as follows:

$$R^C(g) = R^E_{R^D_g(E(g))}\left(D\left(R^D_g(E(g))\right)\right) \tag{17}$$

where g denotes noisy image, E denotes erosion operation, R^E denotes morphological erosion reconstruction, D denotes dilation operation and R^D denotes morphological dilation reconstruction.

Since morphological reconstruction cannot effectively handle the weak edge regions of noisy images, pixel x_i^{MR} in the morphological reconstruction image is corrected by the following equation:

$$\eta_i = \frac{\sum\limits_{r \in N_i^{MR}} \sqrt{\rho_{1r}\rho_{2r}} x_r^{MR}}{\sum\limits_{r \in N_i^{MR}} \sqrt{\rho_{1r}\rho_{2r}}} \tag{18}$$

where ρ_{1r} and ρ_{2r} are weight coefficients. N_i^{MR} denotes the local window centered at pixel x_i^{MR} in the morphological reconstruction image.

To further enhance the robustness of the proposed algorithm to noise, the neighborhood pixel x_r^{MR} whose gray value is closer to the original value in the filtered image should be given a larger value of ρ_{1r}. In general, if the difference between the gray value of a pixel in the noisy image and the corresponding pixel in the filtered image is smaller, it means that this pixel in the noisy image is relatively weakly contaminated by noise. After morphological reconstruction, the filtered value of this pixel is closer to the original value. Therefore, the weight coefficient ρ_{1r} is defined as follows:

$$\rho_{1r} = \left(1 - \sqrt{\frac{\|x_r - x_r^{MR}\|}{255}}\right)^2 \tag{19}$$

where x_r denotes the pixel in local window N_i of the noisy image and x_r^{MR} denotes the pixel in local window N_r^{MR} of the filtered image. The spatial coordinates of pixel x_i^{MR} and pixel x_i correspond.

To improve the detail retention ability of the proposed algorithm, the neighborhood pixel x_r^{MR} with similar gray value to the center pixel x_i^{MR} should be given a larger value of ρ_{2r}. Therefore, the weight coefficient ρ_{2r} is defined as follows:

$$\rho_{2r} = e^{-\frac{\|x_r^{MR} - x_i^{MR}\|^2}{\varphi_i \cdot mean\left(x_r^{MR} - x_i^{MR}\right)}} \tag{20}$$

$$mean\left(x_r^{MR} - x_i^{MR}\right) = \frac{1}{|N_i^{MR}|} \sum_{r \in N_i^{MR}} \|x_r^{MR} - x_i^{MR}\|^2 \tag{21}$$

where $|N_i^{MR}|$ denotes the number of pixels in local window $|N_i^{MR}|$, φ_i is used to control the decay rate of ρ_{2r}.

In this paper, the value of φ_i can be calculated adaptively. According to whether the pixel x_i^{MR} is in the boundary region, φ_i is calculated as follows:

$$\varphi_i = \ln\left\{ 1 + \frac{\left[255 - \left(\max\left(N_i^{MR}\right) - \min\left(N_i^{MR}\right)\right)\right]}{2 * std\left(N_i^{MR}\right)} \right\} \quad (22)$$

where $\max\left(N_i^{MR}\right)$ and $\min\left(N_i^{MR}\right)$ denote the maximum and the minimum gray value of the pixels in N_i^{MR}, respectively. $std\left(N_i^{MR}\right)$ denotes the standard deviation of pixels in N_i^{MR}.

According to Eq. (22), when pixel x_i^{MR} is located in the boundary region, there may be pixels belonging to other clusters in its neighborhood. The gray values of these pixels may differ significantly, i.e., $\max\left(N_i^{MR}\right) - \min\left(N_i^{MR}\right)$ is larger, resulting in φ_i being smaller and ρ_{2r} decays faster, preventing a larger ρ_{2r} from being given to the pixel belonging to other clusters. When pixel x_i^{MR} is located in the flat region, both $\max\left(N_i^{MR}\right) - \min\left(N_i^{MR}\right)$ and $std\left(N_i^{MR}\right)$ are smaller. Considering the trend of logarithmic function, φ_i can be prevented from being too large. At this time, the decay rate of ρ_{2r} is slower, a larger ρ_{2r} will be given to the neighborhood pixel.

The gray value of pixel x_i^{MR} in the morphological reconstruction image is corrected to η_i by Eq. (18). If the gray value of neighborhood pixel x_r in the noisy image is closer to the corrected value η_i, the reliability of x_r is higher. Therefore, in this paper, the reliability w_r of pixel x_r is defined as:

$$w_r = e^{-\frac{\|x_r - \eta_i\|^2}{\tau_i \cdot mean(x_r - \eta_i)}} \quad (23)$$

$$mean\left(x_r - \eta_i\right) = \frac{1}{|N_i|} \sum_{r \in N_i} \|x_r - \eta_i\|^2 \quad (24)$$

where τ_i is used to control the decay rate of w_r. Due to the influence of noise, when there are many pixels in local window N_i with gray values that differ from the corrected value η_i, τ_i should be smaller to accelerate the decay of w_r, so as to prevent higher reliability from being given to some neighborhood pixels. Thus, in this paper, τ_i is defined as:

$$\tau_i = \ln\left(1 + \sqrt{\frac{|N_i|}{\sum_{r \in N_i} \|x_r - \eta_i\|}} \right) \quad (25)$$

In Eq. (25), the logarithmic function is also used to prevent τ_i from being too large.

Fig. 4 illustrates the process of calculating the noise probability p_{i0}. It can be seen from Fig. 4 that although morphological reconstruction smooths most of the noise pixels, some noise pixels are over-preserved in the boundary region of the image. After correction by Eq. (18), it can be seen that the over-preserving phenomenon is decreased.

3.1.2 Distance metric between the pixel and the singleton cluster

In Fig. 4, there are some over-preserved noise blocks in the corrected image, which is due to the uncertainty of the noise resulting in the intensity and position distribution of the noise pixels being random in the noisy image. As a result, there may be a large number of noise pixels with high intensity in a local window of the image. Therefore, it is imprecise to calculate the probability that the central pixel is a noise point only by using the local information of the image, which will result in the pixels in these noise blocks not being assigned to the noise cluster based on the noise distance.

A reasonable method is to introduce the non-local information of the pixel into the distance metric, so the distance between pixel x_i and singleton cluster ω_j is defined as follows:

$$d_{sij}^2 = \kappa_i \left[(1 - p_{i0}) \|x_i - v_j\|^2 + p_{i0} \|\eta_i - v_j\|^2 \right] + (1 - \kappa_i) \|\eta_i^{nl} - v_j\|^2 \quad (26)$$

where η_i^{nl} denotes the non-local information of pixel x_i, v_j denotes the center of singleton cluster ω_j and κ_i denotes the reliability of local window N_i centered at pixel x_i.

The formula for exploiting the non-local information of pixel x_i is as follows:

$$\eta_i^{nl} = \frac{\sum_{\substack{r \in W_i^S \\ r \neq i}} z_{ir} \eta_r}{\sum_{\substack{r \in W_i^S \\ r \neq i}} z_{ir}} \quad (27)$$

$$z_{ir} = e^{-\frac{\left\| \eta\left(W_i^R\right) - \eta\left(W_r^R\right) \right\|_\sigma^2 + (1 - p_{i0})\|\eta_i - \eta_r\|^2}{h^2}} \quad (28)$$

$$h = \frac{1}{n} \sum_{i=1}^{n} std\left(N_i\right) \quad (29)$$

where η_i is obtained by Eq. (18) and W_i^S denotes the search window of size $S \times S$ centered at pixel η_i in the corrected image. $\eta\left(W_i^R\right)$ is the gray vector set of pixels in local window W_i^R of size $R \times R$ centered at pixel η_i. $\left\| \eta\left(W_i^R\right) - \eta\left(W_r^R\right) \right\|_\sigma^2$ is Gaussian weighted squared Euclidean distance between two local windows.

In Eq. (28), the smaller the noise probability p_{i0}, the more accurate the gray value of center pixel η_i. When measuring the difference between two local windows, the weight of the gray difference between central pixels should be increased. $std\left(N_i\right)$ denotes the standard deviation of local window N_i in the noisy image. When the image to be segmented is heavily contaminated by noise, h increases with $std\left(N_i\right)$, so the pixels in the search window have more influence on center pixel η_i to enhance the denoising ability.

In order to reasonably utilize the non-local information of the image, making the algorithm to be more robust to
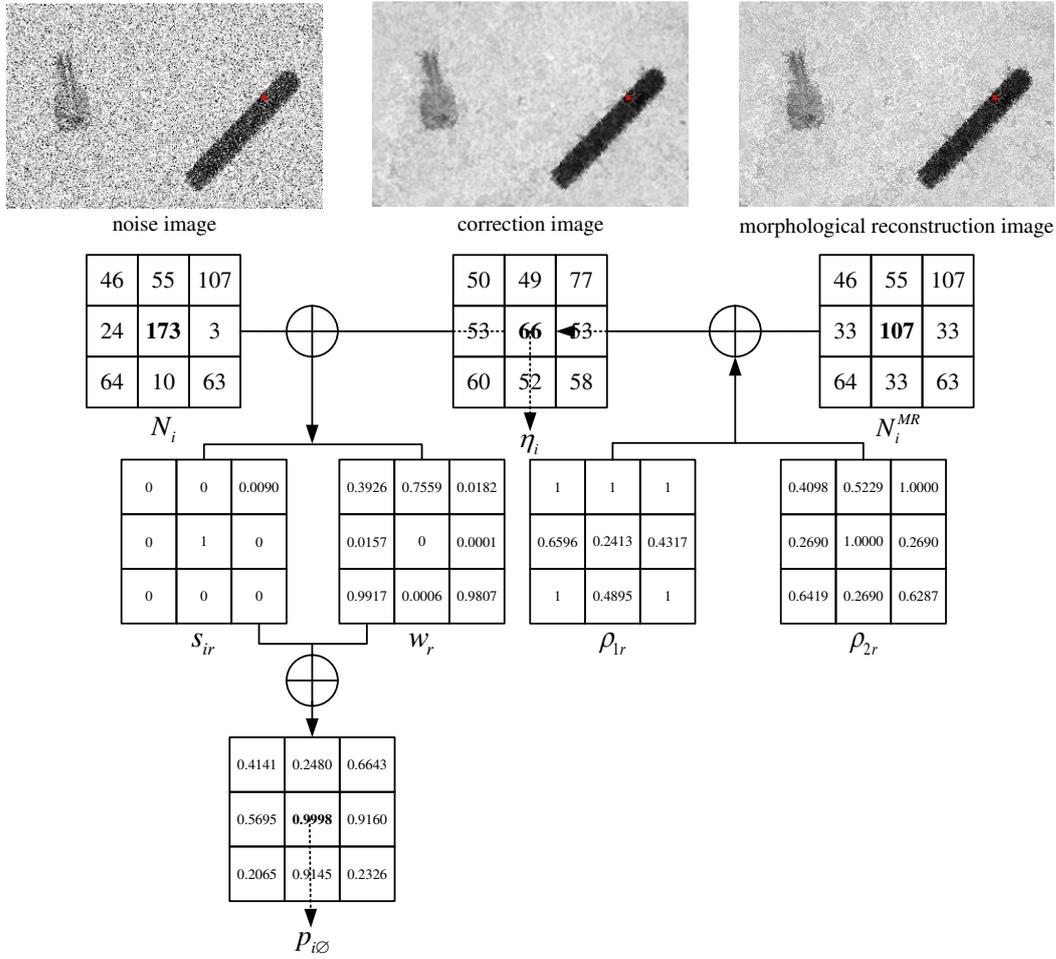
46	55	107
24	**173**	3
64	10	63

N_i

50	49	77
53	**66**	63
60	52	58

η_i

46	55	107
33	**107**	33
64	33	63

N_i^{MR}

0	0	0.0090
0	1	0
0	0	0

s_{ir}

0.3926	0.7559	0.0182
0.0157	0	0.0001
0.9917	0.0006	0.9807

w_r

1	1	1
0.6596	0.2413	0.4317
1	0.4895	1

ρ_{1r}

0.4098	0.5229	1.0000
0.2690	1.0000	0.2690
0.6419	0.2690	0.6287

ρ_{2r}

0.4141	0.2480	0.6643
0.5695	**0.9998**	0.9160
0.2065	0.9145	0.2326

$p_{i\varnothing}$

Fig. 4 The process of calculating the noise probability p_{i0}

noise while also having better detail retention ability. In this paper, the reliability κ_i of local window N_i is calculated adaptively by the following formula:

$$\kappa_i = e^{-\frac{\left\| mean(N_i) - mean\left(W_i^R\right) \right\| + \left\| std(N_i) - std\left(W_i^R\right) \right\|}{mean\left(N_i - W_i^R\right)}} \tag{30}$$

where $mean\,(N_i)$ and $mean\left(W_i^R\right)$ denote the mean values of local window N_i in the noisy image and local window W_i^R in the corrected image, respectively. $std\,(N_i)$ and $std\left(W_i^R\right)$ denote the standard deviations of N_i and W_i^R, respectively. $mean\left(N_i - W_i^R\right)$ denotes the mean value of the absolute gray difference of the corresponding pixels in N_i and W_i^R.

It can be found from Eq. (30) that if the difference between the standard deviation and mean value of local window N_i in the noisy image and local window W_i^R in the corrected image is smaller, it means that the two local windows are more similar and the reliability of N_i is higher.

In summary, when reliability κ_i of N_i is high, d_{sij}^2 depends mainly on $\left\| x_i - v_j \right\|^2$ if noise probability p_{i0} is low, otherwise d_{sij}^2 depends mainly on $\left\| \eta_i - v_j \right\|^2$. When the reli-

ability κ_i is low, d_{sij}^2 depends mainly on $\left\| \eta_i^{nl} - v_j \right\|^2$. Therefore, the original, local and non-local information of pixels is fully used to calculate the distance between the pixel and the singleton cluster.

3.1.3 Distance metric between the pixel and the meta-cluster

In ECM, when the centers of single clusters contained in a meta-cluster are closer to the barycenter of this meta-cluster, an unreasonable clustering result may be generated. In fact, the distance between pixel x_i and meta-cluster A_j depends not only on the distance between the pixel and the barycenter $\overline{v_j}$, but also on the distance between the pixel and all singleton clusters ω_k contained in meta-cluster A_j. Therefore, the CCM algorithm solves the above problem to some extent by defining a new metric formula to calculate the distance between object x_i and meta-cluster $A_j(\left| A_j \right| > 1)$. However, there is a parameter that needs to be manually selected in this distance metric. In order to avoid the influence of manually selecting the parameter on the performance of the al-

gorithm, an adaptive parameter selection method is designed in this paper. The distance between pixel x_i and meta-cluster A_j is defined as follows:

$$d_{mij}^2 = \frac{\sum\limits_{\omega_k \in A_j} d_{sik}^2 + \chi_i d_{sij}^2}{|A_j| + \chi_i} \tag{31}$$

where d_{sik} denotes the distance between pixel x_i and the center of singleton cluster ω_k, d_{sij} denotes the distance between pixel x_i and the barycenter of meta-cluster A_j. The barycenter $\overline{v_j}$ is obtained by Eq. (6) and Eq. (7). χ_i is an adaptive weight parameter.

In an image, it is difficult to assign the pixels in the boundary region to a specific singleton cluster. It is more reasonable to assign these pixels with high uncertainty to the meta-cluster. In CCM, the author considers that a larger χ_i will make object x_i have a higher probability to be assigned to the meta-cluster. Therefore, the pixels in the boundary region should have a large χ_i. By analyzing the characteristics of the pixels in the boundary region, it can be seen that these pixels may assign similar membership degrees to singleton clusters that are close to them, so the classification of pixels is ambiguous, i.e., the entropy of membership degree is large. Thus, in this paper χ_i is defined by the concept of entropy as follows:

$$\chi_i = H(BetP_i) \tag{32}$$

where $BetP_i$ is obtained by Eq. (1), which denotes the membership degree of pixel x_i belonging to singleton clusters, $H(BetP_i)$ denotes the Shannon entropy of $BetP_i$.

3.1.4 Minimization of the objective function

In summary, the objective function of this paper is defined as follows:

$$J = \sum_{i=1}^{n} \sum_{\{j|A_j \subseteq \Omega\}} m_{ij}^\beta D_{ij}^2$$
$$D_{ij}^2 = \begin{cases} \delta_i^2, & A_j = \emptyset \\ d_{sij}^2, & |A_j| = 1 \\ d_{mij}^2, & |A_j| > 1 \end{cases} \tag{33}$$

where δ_i, d_{sij} and d_{mij} denote the distance between pixel x_i and the noise cluster, singleton cluster and meta-cluster, respectively.

By minimizing J, credal partition matrix $M = \{m_1, \cdots, m_n\}$ and cluster center matrix V can be obtained. Using the constraint $\sum\limits_{\{j|A_j \subseteq \Omega\}} m_{ij} = 1$, Lagrange function L is given as:

$$L(M, \lambda_1, \cdots, \lambda_n) = J - \sum_{i=1}^{n} \lambda_i \left(\sum_{\{j|A_j \subseteq \Omega\}} m_{ij} - 1 \right) \tag{34}$$

Considering that V is fixed, let the partial derivatives of L with respect to m_{ij} and λ_i be zero, we obtain:

$$\frac{\partial L}{\partial m_{ij}} = \beta m_{ij}^{\beta-1} D_{ij}^2 - \lambda_i = 0 \tag{35}$$

$$\frac{\partial L}{\partial \lambda_i} = \sum_{\{j|A_j \subseteq \Omega\}} m_{ij} - 1 = 0 \tag{36}$$

From Eq. (35), we obtain:

$$m_{ij} = \left(\frac{\lambda_i}{\beta} \right)^{\frac{1}{\beta-1}} \left(\frac{1}{D_{ij}^2} \right)^{\frac{1}{\beta-1}} \tag{37}$$

Using Eq. (36) and Eq. (47), we obtain:

$$\left(\frac{\lambda_i}{\beta} \right)^{\frac{1}{\beta-1}} = \frac{1}{\sum\limits_{\{j|A_j \subseteq \Omega\}} D_{ij}^{\frac{-2}{\beta-1}}} \tag{38}$$

Using Eq. (37) and Eq. (38), we obtain:

$$m_{ij} = \frac{D_{ij}^{\frac{-2}{\beta-1}}}{\sum\limits_{\{k|A_k \subseteq \Omega\}} D_{ik}^{\frac{-2}{\beta-1}}} \tag{39}$$

Using Eq. (39), we can get the detailed mass of belief respectively on noise cluster, singleton cluster and meta-cluster as follows:

$$m_{i\emptyset} = \frac{\delta^{\frac{-2}{\beta-1}}}{\sum D}, \ A_j = \emptyset \tag{40}$$

$$m_{ij} = \frac{d_{sij}^{\frac{-2}{\beta-1}}}{\sum D}, \ |A_j| = 1 \tag{41}$$

$$m_{ij} = \frac{d_{mij}^{\frac{-2}{\beta-1}}}{\sum D}, \ |A_j| > 1 \tag{42}$$

where $\sum D$ is defined as follows:

$$\sum D = \sum_{A_j = \emptyset} \delta^{\frac{-2}{\beta-1}} + \sum_{|A_j|=1} d_{sij}^{\frac{-2}{\beta-1}} + \sum_{|A_j|>1} d_{mij}^{\frac{-2}{\beta-1}} \tag{43}$$

Considering that M is fixed, the partial derivatives of J with respect to v_l are obtained by:

$$\frac{\partial J}{\partial v_l} = \sum_{i=1}^{n} \sum_{A_l \cap A_j \neq \emptyset} m_{ij}^\beta \frac{\partial D_{ij}^2}{\partial v_l} \tag{44}$$

with

$$\frac{\partial D_{ij}^2}{\partial v_l} = 2(\xi_i - v_l), \ |A_l| = 1 \tag{45}$$

$$\frac{\partial D_{ij}^2}{\partial v_l} = \frac{2(\xi_i - v_l) + \frac{2\chi_i}{|A_j|} \left(\xi_i - \frac{\sum_{\omega_g \in A_j} v_g}{|A_j|} \right)}{|A_j| + \chi_i}, \ A_l \in A_j, |A_j| > 1 \tag{46}$$

Thus,

$$\frac{\partial J}{\partial v_l} = \sum_{i=1}^{n} 2m_{il}^{\beta} (\zeta_i - v_l)$$
$$+ \sum_{i=1}^{n} \sum_{A_l \in A_j} m_{ij}^{\beta} \frac{2(\xi_i - v_l) + \frac{2\chi_i}{|A_j|} \left(\xi_i - \frac{\Sigma_{\omega_g \in A_j} v_g}{|A_j|} \right)}{|A_j| + \chi_i} \qquad (47)$$

with,

$$\xi_i = \kappa_i \left[(1 - p_{i\emptyset}) x_i + p_{i\emptyset} \eta_i \right] + (1 - \kappa_i) \eta_i^{nl} \qquad (48)$$

Letting these partial derivatives be zero obtains c linear equations:

$$\sum_{i=1}^{n} m_{il}^{\beta} \zeta_i + \sum_{i=1}^{n} \sum_{A_l \in A_j} m_{ij}^{\beta} \frac{1 + \frac{\chi_i}{|A_j|}}{|A_j| + \chi_i} \zeta_i$$
$$= \sum_{i=1}^{n} m_{il}^{\beta} v_l + \sum_{i=1}^{n} \sum_{A_l \in A_j} m_{ij}^{\beta} \frac{v_l + \frac{\chi_i \Sigma_{\omega_g \in A_j} v_g}{|A_j|^2}}{|A_j| + \chi_i} \qquad (49)$$

The system of linear equations can be represented as:

$$B_{c \times n} X_{n \times 1} = H_{c \times c} V_{c \times 1} \qquad (50)$$

where the elements in these matrices are obtained as follows:

$$B_{li} = m_{il}^{\beta} + \sum_{A_l \in A_j} m_{ij}^{\beta} \frac{1 + \frac{\chi_i}{|A_j|}}{|A_j| + \chi_i} \qquad (51)$$

$$H_{ll} = \sum_{i=1}^{n} m_{il}^{\beta} + \sum_{i=1}^{n} \sum_{A_l \in A_j} m_{ij}^{\beta} \frac{1 + \frac{\chi_i}{|A_j|^2}}{|A_j| + \chi_i} \qquad (52)$$

$$H_{lq} = \sum_{i=1}^{n} \sum_{A_l \in A_k, A_q \in A_k} m_{ik}^{\beta} \frac{\chi_i}{|A_k|^2 (|A_k| + \chi_i)}, \, l \neq q \qquad (53)$$

V is the solution of the linear equation system (50) and the solution procedure is as follows:

$$V_{c \times 1} = H_{c \times c}^{-1} B_{c \times n} X_{n \times 1} \qquad (54)$$

3.2 Specifying meta-clusters

Since there are pixels belonging to the meta-cluster and the noise cluster in the credal partition, in order to obtain the final segmentation image, it is necessary to specify meta-clusters and recover the noise cluster. Therefore, this section proposes a method for specifying meta-clusters based on Dempster's rule of combination.

Let x_i be a pixel belonging to a meta-cluster and there are pixels belonging to both the singleton cluster and the meta-cluster in its neighborhood.

First, the size of the local window of pixel x_i can be determined adaptively. Let $\left| N_i^{a \times a} \right|$ denote the number of singleton clusters in local window $\left| N_i^{a \times a} \right|$ of size $a \times a$ centered at pixel x_i. As the size of the window increases, if the

number of the singleton cluster in the window is constant, it means that the local window is a block containing complete cluster information and pixel x_i can be specified by using the cluster information. Therefore, if the size of the window satisfies the following conditions, set it to $a \times a$.

$$\left| N_i^{(a+2) \times (a+2)} \right| = \left| N_i^{a \times a} \right|, \, a \geq 3 \qquad (55)$$

where a is an odd number. To prevent a from being large, let $a \leq 9$.

After determining the size of local window $N_i^{a \times a}$, Eq. (56) is used to recalculate the mass of belief of all pixels belonging to the singleton cluster and the meta-cluster in $N_i^{a \times a}$, thereby the mass of belief on the noise cluster is equally reassigned to all clusters except the noise cluster.

$$r \in N_i^{a \times a}, \forall A_j \subseteq \Omega$$
$$m_{rj}' = \begin{cases} m_{rj} + \frac{m_{r\emptyset}}{2c-1}, & A_j \neq \emptyset \\ 0, & A_j = \emptyset \end{cases} \qquad (56)$$

Then, m' of all the pixels belonging to the meta-cluster in $N_i^{a \times a}$ are combined using Dempster's rule of combination as follows:

$$m_{ij}^{\cap} = \left(m_1' \oplus \cdots \oplus m_{nc}' \right) (A_j), \, \forall A_j \subseteq \Omega, A_j \neq \emptyset \qquad (57)$$

where $m_{ij}^{\cap}$ denotes the mass of belief of center pixel x_i belonging to cluster A_j after combination. Dempster's rule of combination satisfies associative law, so Eq. (2) can be used to combine successively.

Next, the local spatial information is used to correct m' of pixels belonging to the singleton cluster in $N_i^{a \times a}$ as follows:

$$r \in N_i^{a \times a}, \forall A_j \subseteq \Omega, A_j \neq \emptyset$$
$$m_{rj}'' = \begin{cases} \frac{1}{d_r} m_{rj}', & A_j \neq \Omega \\ 1 - \frac{1}{d_r} + \frac{1}{d_r} m_{rj}', & A_j = \Omega \end{cases} \qquad (58)$$

where d_r denotes the spatial Euclidean distance between the neighborhood pixel belonging to the singleton cluster and center pixel x_i.

Finally, $m_i^{\cap}$ is combined with m'' of all pixels belonging to the singleton cluster in $N_i^{a \times a}$ as follows:

$$m_{ij}^{\odot} = \left(m_i^{\cap} \oplus m_1'' \oplus \cdots \oplus m_{nc}'' \right) (A_j), \, \forall A_j \subseteq \Omega, A_j \neq \emptyset \quad (59)$$

where $m_{ij}^{\odot}$ denotes the mass of belief of center pixel x_i belongings to cluster A_j.

In order to assign pixel x_i to a specific singleton cluster, $m_{ij}^{\odot}$ is transformed into $BetP_i(\omega_j)$ by Eq. (1) and $BetP_i(\omega_j)$ is considered as the membership degree of pixel x_i belonging to specific singleton cluster ω_j. In addition, the maximum membership principle is used to determine the classification of pixel x_i.

3.3 Recovering the noise cluster

In order to assign the pixels belonging to the noise cluster to a specific singleton cluster, this section proposes a method for recovering the noise cluster. When pixel x_i belongs to the noise cluster, it means that the gray value of this pixel has been severely corrupted by noise. It is necessary to use the spatial information of this pixel to recalculate the gray value to improve the accuracy of image segmentation.

First, the gray value of pixel x_i is recalculated as follows:

$$\xi_i = \kappa_i \cdot \eta_i + (1 - \kappa_i) \cdot \eta_i^{nl} \tag{60}$$

where η_i, η_i^{nl} and κ_i are obtained by Eq. (18), Eq. (27) and Eq. (30), respectively.

Since pixel x_i has the maximum mass of belief on the noise cluster, the mass of belief of pixel x_i needs to be recalculated by Eq. (61).

$$m_{ij}' = \frac{d_{ij}^{-2/(\beta-1)}}{\sum_{A_k \subseteq \Omega, A_k \neq \emptyset} d_{ik}^{-2/(\beta-1)}} \tag{61}$$

where d_{ij} denotes the Euclidean distance between pixel ξ_i and cluster A_j.

Then, the size of the local window is determined adaptively by using the method proposed in Section 3.2. Next, Eq. (56) and Eq. (58) are used to correct m of all pixels belonging to the singleton cluster in the local window to obtain m''. Finally, m_i' and m'' are combined as follows:

$$m_{ij}^{\odot} = \left(m_i' \oplus m_1'' \oplus \cdots \oplus m_{nc}'' \right)(A_j), \forall A_j \subseteq \Omega, A_j \neq \emptyset \tag{62}$$

As in Section 3.2, $m_{ij}^{\odot}$ is transformed into $BetP_i(\omega_j)$ by Eq. (1) and $BetP_i(\omega_j)$ is considered as the membership degree of pixel x_i belonging to specific singleton cluster ω_j. Then, the maximum membership principle is used to determine the classification of pixel x_i.

Through the above analysis, the flow of the algorithm proposed in this paper is as follows:

4 Experiments

In order to objectively analyze the performance of the proposed algorithm, this section is presented in six parts. The first part introduces the comparison algorithms and the experimental parameters. The second part introduces the evaluation indexes used in the experiment. In the third part, three synthetic images with size of 256×256 are constructed and used in the experiment. In the fourth part, images from Weizmann segmentation evaluation database [31] and Berkeley Segmentation Dataset and Benchmark (BSDS) [32] are used in the experiment. In the third and fourth parts, evaluation indexes are calculated utilizing the ground truth, which are

Algorithm 1 A robust evidence c-means clustering combining spatial information for image segmentation algorithm

1: Set the number of clusters c, exponent β, minimum error ε and maximum number of iterations T.
2: Set iteration number $t = 1$, initialize randomly cluster center matrix $V^{(t)}$ and credal partition matrix $M^{(t)}$, the centers in $V^{(t)}$ are sorted according to the values of the cluster centers, and the barycenter of the meta-cluster is obtained using Eq. (6) and Eq. (7).
3: Using Eq.(15) to calculate similarity s_{ir} between center pixel x_i and neighborhood pixel x_r, using Eq. (23) to calculate reliability w_r of neighborhood pixel x_r.
4: Using Eq. (14) to calculate noise probability $p_{i\emptyset}$.
5: Using Eq. (13) to calculate noise distance δ_i.
6: Using Eq. (26) to calculate distance d_{sij}^2 between pixel x_i and singleton cluster ω_j.
7: Using Eq. (31) to calculate distance d_{mij}^2 between pixel x_i and meta-cluster A_j.
8: Using Eqs. (40) - (42) to update credal partition matrix $M^{(t+1)}$.
9: Using Eq. (54) to update cluster center matrix $V^{(t+1)}$.
10: If $\left\| V^{(t+1)} - V^{(t)} \right\| < \varepsilon$ or iteration number $t > T$, then end the iteration. Otherwise, let $t = t + 1$, return to step 6.
11: After obtaining $V^{(t)}$ and $M^{(t)}$, using Eq. (55) to adaptively determined the size of the local window for pixels belonging to the meta-cluster and the noise cluster.
12: Using Eqs. (56) - (59) to update the basic belief assignment for pixels belonging to the meta-cluster.
13: Using Eqs. (56), (58) and (60) - (62) to update the basic belief assignment for pixels belonging to the noise cluster.
14: The updated basic belief assignment is transformed into the membership degree using Eq (1), and using the maximum membership principle to determine the classification of pixel x_i.

used to compare the segmentation performance of algorithms. In the fifth part, Synthetic Aperture Radar (SAR) [33] images are used in the experiment. Since there is no ground truth in the SAR database, the segmentation performance and robustness of algorithms are compared by clustering validity index, image quality evaluation index and visual effect. Finally, the average number of iterations and the average running time of algorithms on the selected synthetic images, real images and SAR images are shown in the form of histograms, the efficiency of algorithms is objectively estimated. The experimental environment is Windows 11, Intel Core i7-10875H, 32G RAM, MATLAB R2020a.

4.1 Comparison algorithms and parameters setting

The proposed algorithm is compared with two clustering algorithms based on evidence theory and seven clustering algorithms based on fuzzy theory. The two clustering algorithms based on evidence theory are ECM [19] and DEC [23]. The seven clustering algorithms based on fuzzy theory are FCM_S1 [12], FCM_S2 [12], FLICM [14], FCM_NLS [13], FRFCM [15], FCM_SICM [16], and IFLICMLNLI [18].

In ECM, set penalization exponent $\alpha = 2$ according to [19]. In DEC, the meta-cluster threshold is set to 0.3 accord-

ing to [23]. Exponent β and the noise distance parameter λ in ECM and DEC are set to 2 and 0.5, respectively. The fuzzy exponent in all fuzzy clustering algorithms is set to 2. In FCM_S1 and FCM_S2, the weight coefficient of the local spatial constraint term is set to 6 according to [12]. In FCM_NLS, the weight coefficient of the non-local spatial constraint term is set to 6 and the size of the search window is set to 21×21 according to [13]. In FRFCM, set a 3×3 square structuring element for morphological reconstruction and set a 3×3 median filter window. In FCM_SICM, set $\sigma_d = 3.5$, $\sigma_r = 3.5$ according to [16]. In FCM_S1, FCM_S2, FLICM, FCM_NLS, FCM_SICM and the proposed algorithm, the size of the local window is set to 3×3. In IFLICMLNLI, since the size of the local window and the search window are the same, set the size of both to 5×5. In the proposed algorithm, the size of the search window is set to 7×7 and set a 3×3 square structuring element for morphological reconstruction.

4.2 Evaluation indexes

In order to objectively and quantitatively compare the segmentation and anti-noise performance of algorithms, Segmentation Accuracy (SA) [11], Normalized Mutual Information (NMI) [34], Mean Intersection-over-Union (mIoU) [35], Adjusted Rand index (ARI) [36], Peak Signal-to-Noise Ratio (PSNR) [37], Partition Coefficient (V_{pc}) [38] and Partition Entropy (V_{pe}) [39] are used to evaluate the image segmentation results of the proposed algorithm and nine comparison algorithms. The calculation formula of above evaluation indexes are as follows:

$$SA = \sum_{i=1}^{c} \frac{|B_i \cap C_i|}{\sum_{j=1}^{c} C_j} \tag{63}$$

where B_i denotes the set of pixels belonging to the ith cluster in the segmentation result, C_i denotes the set of pixels belonging to ith cluster in the ground truth, c is the number of clusters. The larger the value of SA, the better segmentation result.

$$NMI = \frac{2MI(I_1;I_2)}{H(I_1) + H(I_2)} \tag{64}$$

where I_1 denotes the category label image of segmentation result, I_2 denotes the category label image of ground truth. $MI(I_1;I_2)$ is the mutual information of I_1 and I_2, $H(I_1)$ and $H(I_2)$ are the entropy of I_1 and I_2. The larger the value of NMI, the closer the segmentation result is to the ground truth.

$$mIoU = \frac{1}{c} \sum_{i=1}^{c} \frac{|B_i \cap C_i|}{|B_i \cup C_i|} \tag{65}$$

where B_i, C_i and c have the same meaning as in Eq. (63). The larger the value of mIoU, the better segmentation result.

$$ARI = \frac{RI - E[RI]}{\max(RI) - E[RI]} \tag{66}$$

$$RI = \frac{a+b}{n(n-1)/2} \tag{67}$$

where a denotes the number of pairs of pixels that belong to the same cluster both in the segmentation result and in the ground truth. b denotes the number of pairs of pixels that belong to different clusters both in the segmentation result and in the ground truth. n is the number of pixels, RI is the Rand index and $E(RI)$ denotes the expected value of the Rand index. The larger the value of ARI, the better the clustering performance of the algorithm.

$$PSNR = 10\log_{10}\left[\frac{(L-1)^2}{MSE}\right] \tag{68}$$

where L denotes the gray level of the image, MSE denotes the mean square error of the segmentation result and the ground truth. The larger the value of PSNR, the better the image segmentation quality of the algorithm.

$$V_{pc} = \frac{\sum_{i=1}^{n} \sum_{j=1}^{c} u_{ij}^2}{n} \tag{69}$$

$$V_{pe} = \frac{-\sum_{i=1}^{n} \sum_{j=1}^{c} u_{ij} \log u_{ij}}{n} \tag{70}$$

where u_{ij} denotes the membership degree of pixel x_i belonging to the jth cluster, n is the number of pixels, c is the number of clusters. The larger the value of V_{pc} and the smaller the value of V_{pe}, the better the clustering performance of the algorithm.

4.3 Results on synthetic images

To demonstrate the anti-noise ability of the proposed algorithm on synthetic images, three synthetic images are constructed in this section. Synthetic image 1 is shown in Fig. 5(a) which contains four clusters with gray values of 0, 100, 170 and 255, respectively. Synthetic image 2 is shown in Fig. 6(a) which contains three clusters with gray values of 0, 75 and 140, respectively. Synthetic image 3 is shown in Fig. 7(a) which contains four clusters with gray values of 0, 75, 185 and 245, respectively. Firstly, Gaussian noise with mean 0 and variance 0.2 is added into each synthetic image, then Salt & Pepper noise with intensity of 20% is added. The noisy synthetic images are shown in Figs. 6(b), 7(b) and 8(b), the segmentation results are shown in Figs. 6(c-l), 7(c-l) and 8(c-l).

It can be seen from Figs. 5, 6, and 7, ECM and DEC are not directly used for noisy image segmentation because the
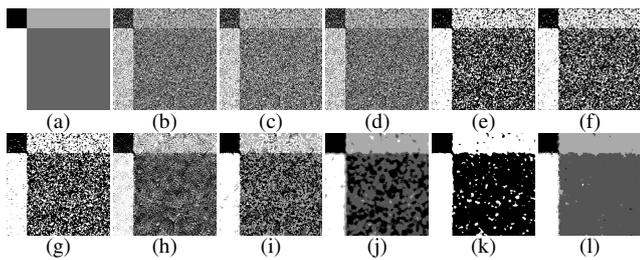
Fig. 5 Segmentation results of synthetic image 1, **a** Ground truth, **b** Image with 20% mixed noise, **c** ECM, **d** DEC, **e** FCM_S1, **f** FCM_S2, **g** FLICM, **h** FCM_NLS, **i** FRFCM, **j** FCM_SICM, **k** IFLICMLNLI and **l** Proposed algorithm

Fig. 6 Segmentation results of synthetic image 2, **a** Ground truth, **b** Image with 20% mixed noise, **c** ECM, **d** DEC, **e** FCM_S1, **f** FCM_S2, **g** FLICM, **h** FCM_NLS, **i** FRFCM, **j** FCM_SICM, **k** IFLICMLNLI and **l** Proposed algorithm

Fig. 7 Segmentation results of synthetic image 3, **a** Ground truth, **b** Image with 20% mixed noise, **c** ECM, **d** DEC, **e** FCM_S1, **f** FCM_S2, **g** FLICM, **h** FCM_NLS, **i** FRFCM, **j** FCM_SICM, **k** IFLICMLNLI and **l** Proposed algorithm

pixels belonging to the noise cluster are not effectively recovered in the segmentation results. Meanwhile, ECM and DEC do not introduce the spatial information of image pixels, a large number of pixels are assigned to the wrong cluster as a result. FLICM only utilizes the local gray and spatial information of pixels, it cannot effectively suppress noise pixels when the noise intensity is high. FCM_S1 and FCM_S2, which introduce the local spatial information of pixels, also cannot achieve satisfactory segmentation results. Although FCM_NLS introduces the non-local spatial information of pixels into the objective function, the denoising performance of non-local mean filtering is limited. In addition, the parameter that controls the spatial information constraint term is a fixed value, which cannot be adaptively calculated according to the characteristics of pixels, resulting in poor segmentation results. FRFCM utilizes morphological reconstruction for filtering, therefore the segmentation results are slightly better than FLICM. For synthetic images 1 and 3, it can be seen from Fig. 5(k) and Fig. 7(k) that IFLICMLNLI has the problem of overlapping cluster centers when high intensity mixed noise is added. For synthetic image 2, when 20% mixed noise is added, IFLICMLNLI can effectively suppress the noise in the right and middle regions of Fig. 6(k), but there are still many noise blocks in the left region. FCM_SICM uses fast bilateral filter to smooth the noise and introduces adaptive weights, which considers not only the spatial and intensity information of the filtered image, but also the original information of the image, so the segmentation results are better than FRFCM. The proposed algorithm uses the noise distance to assign the detected noise points to the noise cluster, which suppresses the influence of noise points on updating the cluster centers. Simultaneously, the spatial information of pixel is utilized to calculate the distance between the pixel and the cluster center, which improves the accuracy of pixel classification. The image segmentation result is better than comparison algorithms.

Next, all algorithms are run on synthetic images corrupted by mixed noise of different intensities. SA, NMI, mIoU, ARI and PSNR are selected to quantitatively evaluate the segmentation results of different algorithms, the numer-
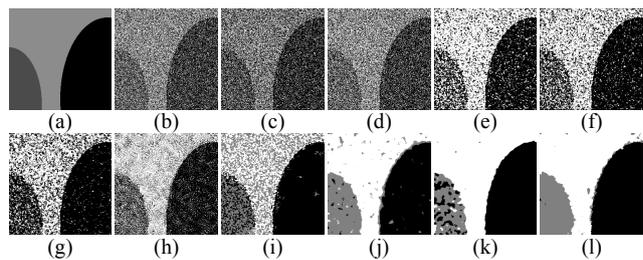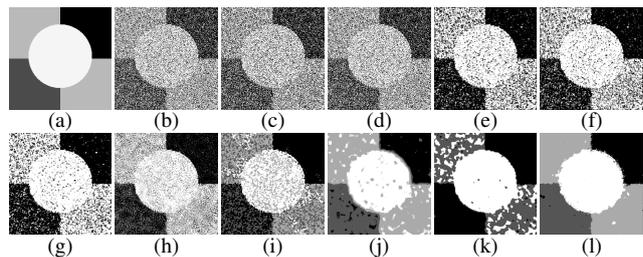
ical results are shown in Table 1-5. In Table 1-5, the steps of adding mixed noise are as follows: Firstly, Gaussian noise with mean 0 and variance 0.01, 0.05, 0.1, 0.15, 0.2 are added into each synthetic image. Then Salt & Pepper noise with intensity of 1%, 5%, 10%, 15%, 20% are added in turn.

Table 1-5 shows that ECM and DEC have lower SA, NMI, mIoU, ARI, and PSNR due to the lack of a recovery method for noise points. FCM_S1 and FCM_S2 introduce local filtering and have similar anti-noise performance in the three synthetic images. When the intensity of mixed noise is lower, FCM_NLS has higher SA, NMI, mIoU, ARI, and PSNR than FCM_S1 and FCM_S2 due to FCM_NLS introducing non-local filtering. However, when the intensity of mixed noise increases, the anti-noise performance of these three algorithms decreases to some extent. FLICM introduces local information and membership of pixels. Although FLICM algorithm has higher SA, NMI, and ARI than other comparison algorithms in synthetic image 1 corrupted by 1% mixed noise, the SA, NMI, mIoU, ARI, and PSNR decrease substantially with the increase of mixed noise intensity in the three synthetic images. FRFCM has the highest SA, NMI, mIoU, ARI, and PSNR in synthetic image 2 and synthetic image 3 corrupted by 1% mixed noise, which is because morphological reconstruction has strong denoising ability when the intensity of mixed noise is low, but the denoising ability of morphological reconstruction gradually decreases with the increase of noise intensity. Although

Table 1 SA of ten algorithms on synthetic images corrupted by mixed noise of different intensities

Image	Mixed noise	ECM	DEC	FCM_S1	FCM_S2	FLICM	FCM_NLS	FRFCM	FCM_SICM	IFLICM LNLI	Proposed
synthetic image 1	1%	0.6364	0.6759	0.7127	0.7363	**0.9993**	0.8095	0.8062	0.9790	0.9833	0.9989
	5%	0.4054	0.5120	0.4152	0.4580	0.4752	0.5232	0.6902	0.7303	0.1989	**0.9946**
	10%	0.3533	0.4017	0.3508	0.4090	0.2524	0.3553	0.6395	0.7159	0.1985	**0.9889**
	15%	0.3073	0.3451	0.3122	0.3819	0.3978	0.3384	0.6034	0.7036	0.2031	**0.9829**
	20%	0.2712	0.2983	0.2751	0.3553	0.1944	0.3093	0.4079	0.7089	0.1950	**0.9769**
synthetic image 2	1%	0.6205	0.8425	0.9821	0.9942	0.9986	0.9954	**0.9993**	0.9822	0.9833	0.9986
	5%	0.5178	0.6146	0.8369	0.8407	0.7958	0.9360	0.9903	0.9803	0.9854	**0.9949**
	10%	0.4881	0.5142	0.7556	0.7534	0.6850	0.7769	0.7677	0.9767	0.9896	**0.9909**
	15%	0.4804	0.4888	0.7066	0.6998	0.6595	0.6943	0.7332	0.9682	**0.9878**	0.9844
	20%	0.4707	0.4757	0.6696	0.6583	0.6417	0.6368	0.7069	0.9519	0.9450	**0.9755**
synthetic image 3	1%	0.7560	0.8761	0.9787	0.9932	0.7313	0.9952	**0.9989**	0.9725	0.9786	0.9984
	5%	0.5385	0.5929	0.7674	0.8021	0.7416	0.9248	0.9849	0.9673	0.9775	**0.9925**
	10%	0.4626	0.4925	0.6139	0.6541	0.6230	0.6952	0.9105	0.9591	0.4604	**0.9871**
	15%	0.4158	0.4354	0.5553	0.5976	0.5792	0.5738	0.7833	0.9417	0.4614	**0.9796**
	20%	0.3878	0.3999	0.5072	0.5504	0.5243	0.5055	0.6250	0.9055	0.4611	**0.9751**

Table 2 NMI of ten algorithms on synthetic images corrupted by mixed noise of different intensities

Image	Mixed noise	ECM	DEC	FCM_S1	FCM_S2	FLICM	FCM_NLS	FRFCM	FCM_SICM	IFLICM LNLI	Proposed
synthetic image 1	1%	0.4212	0.5473	0.6837	0.7344	**0.9941**	0.7737	0.7765	0.9026	0.9180	0.9912
	5%	0.1717	0.2316	0.4404	0.4543	0.4945	0.5365	0.7162	0.6868	0.5828	**0.9639**
	10%	0.0893	0.1184	0.3322	0.3469	0.4027	0.4262	0.5949	0.6729	0.5715	**0.9349**
	15%	0.0667	0.0804	0.2564	0.2726	0.3156	0.2990	0.5218	0.6641	0.5383	**0.9119**
	20%	0.0446	0.0511	0.1887	0.2061	0.2084	0.1850	0.3834	0.6306	0.5498	**0.8844**
synthetic image 2	1%	0.5248	0.6304	0.9178	0.9667	0.9904	0.9737	**0.9945**	0.9216	0.9257	0.9898
	5%	0.2044	0.2736	0.6173	0.6378	0.6411	0.7791	0.9475	0.9151	0.9321	**0.9678**
	10%	0.1137	0.1390	0.4600	0.4741	0.5095	0.5362	0.6154	0.8986	0.9466	**0.9490**
	15%	0.0765	0.0859	0.3453	0.3665	0.4094	0.4087	0.5768	0.8692	**0.9341**	0.9260
	20%	0.0508	0.0581	0.2528	0.2791	0.3231	0.2634	0.5363	0.8232	0.8103	**0.8950**
synthetic image 3	1%	0.5536	0.6938	0.9188	0.9695	0.8207	0.9778	**0.9936**	0.9085	0.9236	0.9902
	5%	0.2673	0.3162	0.6012	0.6407	0.6489	0.8042	0.9407	0.8927	0.9181	**0.9626**
	10%	0.1639	0.1883	0.4713	0.4935	0.5268	0.5397	0.7896	0.8661	0.7949	**0.9403**
	15%	0.1071	0.1201	0.3897	0.4066	0.4474	0.4261	0.6212	0.8211	0.7405	**0.9156**
	20%	0.0775	0.0836	0.3129	0.3315	0.3654	0.3367	0.4975	0.7512	0.6522	**0.8999**

Table 3 mIoU of ten algorithms on synthetic images corrupted by mixed noise of different intensities

Image	Mixed noise	ECM	DEC	FCM_S1	FCM_S2	FLICM	FCM_NLS	FRFCM	FCM_SICM	IFLICM LNLI	Proposed
synthetic image 1	1%	0.3961	0.5363	0.6357	0.6705	**0.9984**	0.7161	0.7156	0.9315	0.9499	0.9974
	5%	0.2452	0.3216	0.2911	0.3284	0.2773	0.4078	0.6466	0.6411	0.1564	**0.9815**
	10%	0.1924	0.2320	0.2347	0.2771	0.1962	0.2532	0.5598	0.6296	0.1479	**0.9691**
	15%	0.1646	0.1928	0.1995	0.2472	0.2142	0.2267	0.4867	0.6222	0.1473	**0.9555**
	20%	0.1438	0.1630	0.1655	0.2179	0.0963	0.1869	0.3053	0.6058	0.1244	**0.9354**
synthetic image 2	1%	0.4236	0.7049	0.9523	0.9839	0.9961	0.9870	**0.9982**	0.9522	0.9551	0.9969
	5%	0.3141	0.4335	0.6732	0.6837	0.6307	0.8444	0.9742	0.9475	0.9605	**0.9871**
	10%	0.2923	0.3333	0.5639	0.5662	0.4897	0.5906	0.6052	0.9386	0.9715	**0.9765**
	15%	0.2875	0.3047	0.5001	0.5011	0.4545	0.4967	0.5632	0.9185	**0.9674**	0.9603
	20%	0.2731	0.2895	0.4510	0.4532	0.4307	0.4294	0.5332	0.8828	0.8479	**0.9384**
synthetic image 3	1%	0.6163	0.7883	0.9573	0.9878	0.5574	0.9906	**0.9982**	0.9438	0.9562	0.9970
	5%	0.3617	0.4244	0.6009	0.6500	0.5489	0.8522	0.9753	0.9355	0.9554	**0.9857**
	10%	0.2893	0.3254	0.4285	0.4713	0.4235	0.5135	0.8670	0.9213	0.3507	**0.9752**
	15%	0.2478	0.2715	0.3750	0.4174	0.3851	0.3927	0.6460	0.8916	0.3363	**0.9616**
	20%	0.2228	0.2394	0.3293	0.3706	0.3315	0.3328	0.4638	0.8312	0.3019	**0.9534**

Table 4 ARI of ten algorithms on synthetic images corrupted by mixed noise of different intensities

Image	Mixed noise	ECM	DEC	FCM_S1	FCM_S2	FLICM	FCM_NLS	FRFCM	FCM_SICM	IFLICM LNLI	Proposed
synthetic image 1	1%	0.3292	0.4323	0.5057	0.5357	**0.9977**	0.6124	0.6093	0.9515	0.9594	0.9967
	5%	0.1113	0.1587	0.2798	0.2738	0.3600	0.3754	0.5087	0.5187	0.4163	**0.9849**
	10%	0.0268	0.0695	0.2272	0.2159	0.3092	0.2990	0.4292	0.5057	0.4165	**0.9684**
	15%	0.0135	0.0385	0.1760	0.1626	0.2373	0.2170	0.3744	0.4947	0.4612	**0.9506**
	20%	0.0058	0.0197	0.1242	0.1160	0.1441	0.1274	0.2244	0.4839	0.6176	**0.9345**
synthetic image 2	1%	0.4586	0.6668	0.9551	0.9851	0.9964	0.9888	**0.9981**	0.9562	0.9588	0.9959
	5%	0.1769	0.2971	0.6642	0.6711	0.6145	0.8510	0.9743	0.9518	0.9642	**0.9857**
	10%	0.1048	0.1529	0.5205	0.5197	0.4812	0.5750	0.5817	0.9430	0.9743	**0.9752**
	15%	0.0739	0.0958	0.4183	0.4146	0.3944	0.4510	0.5463	0.9220	**0.9684**	0.9582
	20%	0.0453	0.0659	0.3307	0.3272	0.3191	0.3182	0.5128	0.8827	0.8767	**0.9359**
synthetic image 3	1%	0.4786	0.6893	0.9436	0.9800	0.7323	0.9865	**0.9967**	0.9294	0.9444	0.9953
	5%	0.2152	0.2681	0.5395	0.5901	0.5750	0.8185	0.9537	0.9139	0.9402	**0.9788**
	10%	0.1415	0.1682	0.3740	0.4016	0.4107	0.4440	0.7517	0.8919	0.7749	**0.9641**
	15%	0.0972	0.1145	0.3115	0.3317	0.3625	0.3365	0.5351	0.8463	0.7113	**0.9432**
	20%	0.0736	0.0846	0.2603	0.2801	0.3157	0.2788	0.3814	0.7592	0.5672	**0.9305**

Table 5 PSNR of ten algorithms on synthetic images corrupted by mixed noise of different intensities

Image	Mixed noise	ECM	DEC	FCM_S1	FCM_S2	FLICM	FCM_NLS	FRFCM	FCM_SICM	IFLICM LNLI	Proposed
synthetic image 1	1%	13.0392	18.6126	20.6682	21.7289	32.3575	21.6306	22.8539	25.8291	26.2693	**35.5927**
	5%	9.3737	12.4439	17.0553	17.7403	17.8593	17.8093	21.3475	20.3011	17.3496	**29.4019**
	10%	8.2384	10.0750	15.2190	16.1359	16.3277	16.1744	19.0284	18.9235	15.6304	**27.0308**
	15%	7.6851	8.9765	14.2829	15.0973	15.0476	14.9826	17.4403	18.0265	14.5740	**25.3435**
	20%	7.2923	8.1672	13.5445	14.1005	12.1865	13.8858	15.4857	16.8876	12.1827	**23.7610**
synthetic image 2	1%	16.4816	19.2559	26.1732	30.3957	31.5675	28.4839	**39.1783**	27.1477	26.7851	35.5039
	5%	11.2583	13.3510	18.4827	20.2132	19.9392	19.9456	29.5163	22.6258	21.5921	**31.0616**
	10%	9.3844	10.1447	15.8032	17.5103	17.8093	16.6702	19.6597	19.1395	18.0916	**29.7870**
	15%	8.3681	8.8133	14.2534	15.9375	16.1428	15.0294	18.5749	17.3604	15.8951	**27.4643**
	20%	7.6192	8.0019	13.1385	14.7693	14.9401	13.7138	17.4597	15.9848	14.1749	**25.8111**
synthetic image 3	1%	16.5162	19.2912	24.5103	29.7864	20.8893	28.5295	**37.4840**	24.8473	25.2683	34.1478
	5%	10.8583	12.6154	16.9086	18.4548	17.6465	19.3239	27.4740	21.0325	20.1820	**28.2361**
	10%	8.9805	10.2872	14.6682	16.2983	16.3773	15.5975	21.8795	18.0618	15.1875	**25.2593**
	15%	7.8674	8.8483	13.0273	14.8732	15.0095	13.8193	18.1825	15.9365	13.5106	**23.7598**
	20%	7.2841	7.9550	11.9729	13.7004	13.6420	12.6574	16.1092	14.6881	12.2636	**22.6401**

FCM_SICM does not have the best result in noisy synthetic images, the performance of this algorithm is more stable in noisy synthetic image 2 and noisy synthetic image 3. With the increase of mixed noise intensity, there is no significant decrease in evaluation indexes. However, in the noisy synthetic image 1, the performance of FCM_SICM algorithm has a more substantial degradation, which is due to the fact that this image contains two clusters with a large difference in the number of pixels. Therefore, FCM_SICM algorithm is more sensitive to images containing unbalanced clusters. IFLICMLNLI has better segmentation results in noisy synthetic image 2. Within a certain range, SA, NMI, mIoU and ARI will increase with the increase of mixed noise intensity, which is due to this algorithm integrating local and non-local information, and increasing the weight of neighborhood information in the distance formula when the intensity of mixed noise increases. IFLICMLNLI algorithm has the highest SA, NMI, mIoU, and ARI when 15% mixed noise is added in synthetic image 2, but the anti-noise performance decreases significantly when 20% mixed noise is added. The stability of this algorithm is poor in noisy synthetic image 1 and noisy synthetic image 3. According to Table 1-5, the proposed algorithm has better results overall. In particular, when the intensity of mixed noise is high, the proposed algorithm has higher SA, NMI, mIoU, ARI and PSNR than comparison algorithms, indicating that the proposed algorithm has stronger robustness to noise on synthetic images.

4.4 Results on real images

In this section, images from Weizmann segmentation evaluation database [31] and BSDS [32] are selected for experiments to demonstrate the segmentation performance of the proposed algorithm on noisy real images.
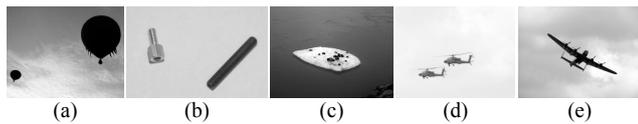
Fig. 8 Images from Weizmann database, **a** _mg_5707, **b** _3076180_cropped, **c** dsc04575, **d** b9vehicles_air015 and **e** bbmf_lancaster_july_06

4.4.1 Results on Weizmann segmentation evaluation database

Five images are selected from Weizmann segmentation evaluation database for experiments. As shown in Fig. 8, which are _mg_5707, _3076180_cropped, dsc04575, b9vehicles_air015 and bbmf_lancaster_july_06, respectively. From left to right in Fig. 8, the images are corrupted by 5%, 5%, 10%, 10% and 15% mixed noise. The noisy images, ground truth and segmentation results are shown in the first row, the last row and the remaining rows of Fig. 9, respectively.

It can be seen from Figs. 9(a) and (c) that when contaminated with mixed noise, especially Gaussian noise, the gray values of the target and the upper part of the background are very close. ECM, DEC, FCM_S1, FCM_S2 and FCM_NLS not only assign a large number of pixels belonging to the upper part of the background to the target, but also have many misclassified pixels in the lower part of the background. The segmentation results of FLICM, FCM_SICM and IFLICMLNLI are slightly better than the above algorithms, but the target region still cannot be segmented. In the segmentation results of the proposed algorithm, although there are a small number of misclassified pixels, the target and background are accurately segmented. Fig. 8(b) contains three clusters. Due to the relatively similar gray value of the left screw and the background, as well as the influence of mixed noise, all comparison algorithms produce incorrect segmentation results. The proposed algorithm successfully identifies the three clusters in the image and produces more accurate segmentation result while suppressing noise pixels. For the aircraft images shown in Fig. 8(d) and (e), in the segmentation results of comparison algorithms except FLICM and IFLICMLNLI, there are a large number of misclassified pixels and the segmentation target is difficult to be identified. FLICM and IFLICMLNLI inaccurately segment the aircraft from the sky. In particular, FLICM segments some of the noise pixels in the sky as aircraft, IFLICMLNLI cannot accurately segment the pixels in the boundary regions, and even incorrectly segments the boundaries of two aircrafts together in Fig. 8(d). The proposed algorithm can effectively segment both the foreground and background in noisy images, and also retains rich details. The segmentation numerical results are shown in Table 6. It can be seen that the evaluation indexes of the proposed algorithm are better than comparison algorithms.
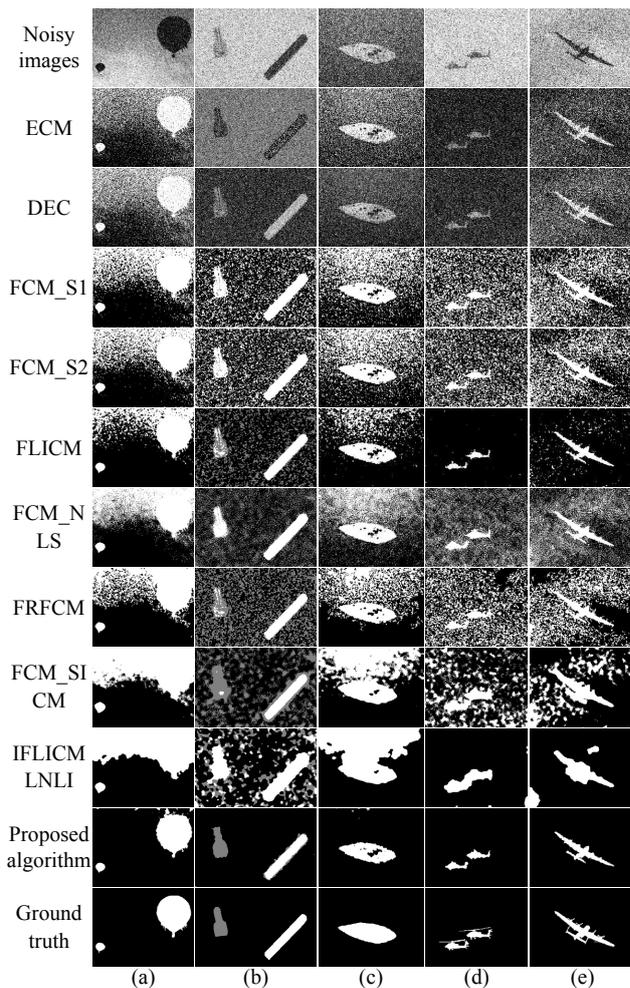

Fig. 9 Segmentation results on images from Weizmann database, **a** _mg_5707 with 5% mixed noise, **b** _3076180_cropped with 5% mixed noise, **c** dsc04575 with 10% mixed noise, **d** b9vehicles_air015 with 10% mixed noise and **e** bbmf_lancaster_july_06 with 15% mixed noise
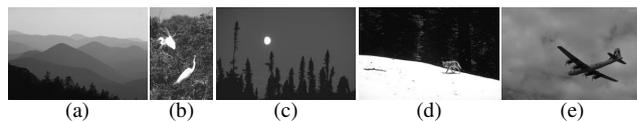

Fig. 10 Images from BSDB, **a** #55067, **b** #311068, **c** #238011, **d** #167062 and **e** #3096

4.4.2 Results on Berkeley Segmentation Dataset and Benchmark

Five images from BSDB are selected for experiments. As shown in Fig. 10, which are #55067, #311068, #238011, #167062 and #3096, respectively. From left to right in Fig. 10, the images are corrupted by 5%, 5%, 10%, 10% and 10% mixed noise. The noisy images, ground truth and segmentation results are shown in the first row, the last row and the remaining rows of Fig. 11, respectively.

Table 6 Quantization results of ten algorithms on real images from Weizmann database

Image	Index	ECM	DEC	FCM_S1	FCM_S2	FLICM	FCM_NLS	FRFCM	FCM_SICM	IFLICM LNLI	Proposed
Fig.9(a)	SA	0.7039	0.6417	0.6997	0.7015	0.8130	0.6937	0.7388	0.6441	0.6846	**0.9777**
	NMI	0.1898	0.1564	0.2279	0.2285	0.3366	0.2234	0.2588	0.1919	0.2178	**0.7878**
	mIoU	0.4785	0.4245	0.4781	0.4797	0.5969	0.4725	0.5155	0.4288	0.4643	**0.9135**
	ARI	0.1526	0.0794	0.1503	0.1527	0.3429	0.1422	0.2071	0.0826	0.1304	**0.8809**
	PSNR	10.4930	12.2872	14.1597	14.3761	15.0627	14.2976	14.9819	14.9552	15.1253	**15.5809**
Fig.9(b)	SA	0.4827	0.4940	0.5994	0.5698	0.7333	0.6588	0.5719	0.7019	0.6403	**0.9806**
	NMI	0.1099	0.1084	0.1687	0.1682	0.3704	0.2991	0.3272	0.3745	0.2314	**0.7941**
	mIoU	0.2396	0.2518	0.2713	0.2623	0.5191	0.3630	0.4610	0.5631	0.3010	**0.8505**
	ARI	0.0745	0.0934	0.1099	0.1012	0.2687	0.2168	0.1727	0.2257	0.1625	**0.8755**
	PSNR	9.8886	12.8429	17.9335	18.3571	23.1901	19.7598	22.5082	23.4797	18.1783	**28.9147**
Fig.9(c)	SA	0.6511	0.5374	0.6412	0.6395	0.8491	0.6592	0.7039	0.6675	0.6556	**0.9847**
	NMI	0.0604	0.0585	0.1056	0.1038	0.2545	0.1170	0.1363	0.1488	0.1541	**0.7771**
	mIoU	0.3983	0.3431	0.4006	0.3991	0.5958	0.4150	0.4506	0.4250	0.4166	**0.9131**
	ARI	0.0668	0.0745	0.0699	0.0684	0.3583	0.0860	0.1297	0.0974	0.0871	**0.8898**
	PSNR	4.1645	5.4228	11.0538	16.1542	16.8094	15.9618	11.8262	17.0338	12.1438	**18.1537**
Fig.9(d)	SA	0.7301	0.6689	0.6147	0.6642	0.9856	0.6923	0.6339	0.7270	0.9595	**0.9882**
	NMI	0.0239	0.0226	0.0463	0.0532	0.5664	0.0625	0.0539	0.0812	0.3988	**0.6323**
	mIoU	0.4216	0.3866	0.3375	0.3673	0.7852	0.3855	0.3497	0.4097	0.6912	**0.8267**
	ARI	0.0608	0.0474	0.0266	0.0441	0.7201	0.0576	0.0341	0.0795	0.5511	**0.7833**
	PSNR	10.0199	10.5686	16.1219	19.8871	19.6993	16.8183	20.1706	16.4291	16.0495	**27.4449**
Fig.9(e)	SA	0.7258	0.6751	0.6121	0.6430	0.9628	0.6787	0.6641	0.7986	0.9426	**0.9887**
	NMI	0.0513	0.0439	0.0718	0.0749	0.4660	0.0855	0.0839	0.1810	0.4502	**0.7595**
	mIoU	0.4187	0.3860	0.3530	0.3708	0.7530	0.3971	0.3875	0.4968	0.7084	**0.8928**
	ARI	0.0837	0.0567	0.0370	0.0525	0.6572	0.0742	0.0656	0.2002	0.5770	**0.8704**
	PSNR	8.1208	9.7149	9.9384	16.0481	17.9373	15.1505	15.6739	15.2481	15.3892	**19.6051**

Table 7 Quantization results of ten algorithms on real images from BSDB

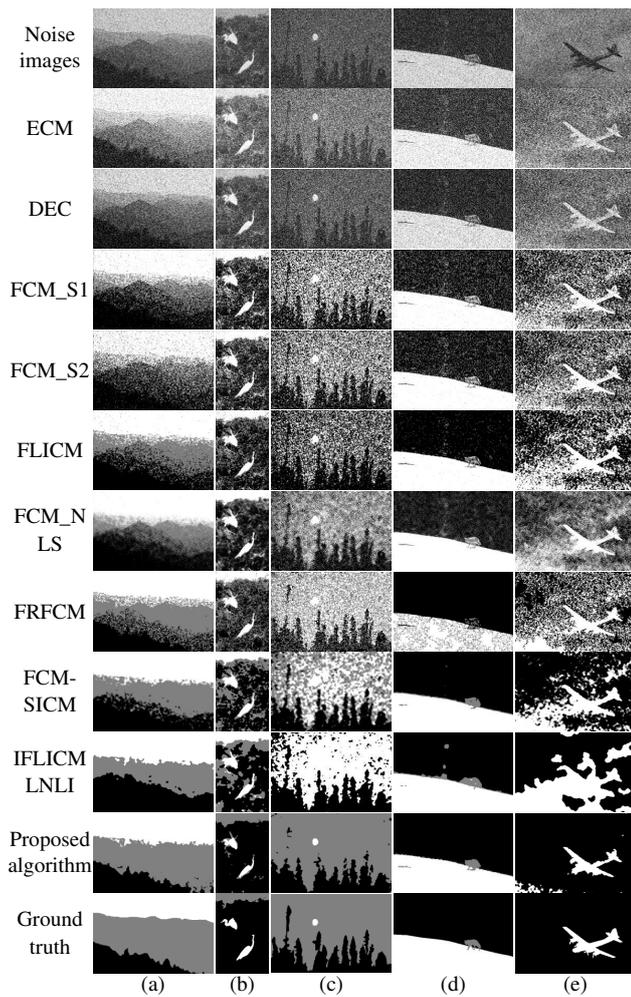| Image	Index	ECM	DEC	FCM_S1	FCM_S2	FLICM	FCM_NLS	FRFCM	FCM_SICM	IFLICM LNLI	Proposed
Fig.11(a)	SA	0.5841	0.6156	0.7116	0.7308	0.7884	0.7318	0.8463	0.8110	0.7748	**0.9256**
	NMI	0.2333	0.2411	0.4825	0.5035	0.5848	0.5279	0.6267	0.6070	0.5848	**0.7627**
	mIoU	0.4132	0.4494	0.5639	0.5855	0.6573	0.5863	0.7293	0.6828	0.6404	**0.8672**
	ARI	0.1720	0.2020	0.3759	0.3992	0.4974	0.4025	0.5885	0.5243	0.4749	**0.7700**
	PSNR	10.2906	12.4696	11.9535	18.3477	19.6905	18.5649	20.1175	20.2699	19.7786	**21.1223**
Fig.11(b)	SA	0.3642	0.4553	0.5309	0.5149	0.5430	0.5603	0.5011	0.5810	0.6039	**0.9542**
	NMI	0.1135	0.1380	0.2862	0.2878	0.3834	0.3793	0.4132	0.4636	0.4484	**0.7017**
	mIoU	0.1708	0.2348	0.2537	0.2484	0.2836	0.2783	0.2721	0.3036	0.3069	**0.8053**
	ARI	0.0313	0.1133	0.2015	0.1991	0.2848	0.2789	0.2879	0.3361	0.3393	**0.8252**
	PSNR	9.4324	12.6919	11.3452	17.6043	13.4123	17.5471	18.6382	18.3753	17.6602	**18.7509**
Fig.11(c)	SA	0.3704	0.4600	0.3044	0.3786	0.4117	0.2868	0.4875	0.6068	0.2728	**0.9418**
	NMI	0.0214	0.0220	0.0848	0.0978	0.1040	0.1091	0.2464	0.4230	0.4771	**0.6532**
	mIoU	0.1889	0.2235	0.1730	0.2132	0.2104	0.1627	0.3100	0.4213	0.2337	**0.8759**
	ARI	0.0044	0.0037	0.0593	0.0597	0.0204	0.0695	0.2242	0.3567	0.5732	**0.7731**
	PSNR	7.7291	10.5185	11.5171	20.4405	20.1639	19.5152	20.1704	21.1478	18.7923	**26.8105**
Fig.11(d)	SA	0.7255	0.7203	0.8015	0.8328	0.9618	0.8298	0.9052	0.9831	0.9740	**0.9905**
	NMI	0.3421	0.3511	0.6955	0.7135	0.8492	0.7320	0.8018	0.9177	0.8972	**0.9364**
	mIoU	0.4440	0.4578	0.5655	0.5848	0.6973	0.5853	0.5977	0.7753	0.7418	**0.8454**
	ARI	0.3659	0.4133	0.6487	0.6856	0.9130	0.6865	0.8706	0.9663	0.9409	**0.9782**
	PSNR	9.4381	10.2615	10.0544	18.5734	18.5363	15.9960	22.1225	15.8508	15.5187	**23.5182**
Fig.11(e)	SA	0.5248	0.5600	0.5697	0.5759	0.5993	0.5741	0.5908	0.7600	0.6821	**0.9684**
	NMI	0.0230	0.0248	0.0619	0.0644	0.0836	0.0694	0.0751	0.1653	0.1276	**0.5464**
	mIoU	0.2964	0.3172	0.3299	0.3340	0.3510	0.3335	0.3446	0.4718	0.4105	**0.7970**
	ARI	0.0021	0.0120	0.0184	0.0213	0.0338	0.0207	0.0289	0.1653	0.0903	**0.7268**
	PSNR	8.9965	11.5911	15.0927	20.1580	18.2374	20.4361	19.1052	21.8718	21.6235	**23.5937**

Fig. 11 Segmentation results on images from BSDB, **a** #55067 with 5% mixed noise, **b** #311068 with 5% mixed noise, **c** #238011 with 10% mixed noise, **d** #167062 with 10% mixed noise and **e** #3096 with 10% mixed noise
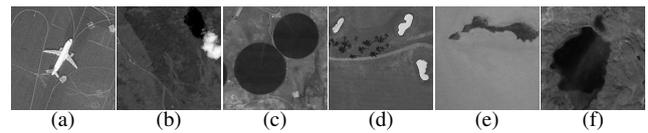

Fig. 12 Images from NWPU-RESISC45 dataset, **a** #airplane_086, **b** #cloud_494, **c** #circular_farmland_130 , **d** #golf_course_332, **e** #island_401 and **f** #lake_103

to the ground truth, all comparison algorithms are unable to segment the moon from the sky. The fourth column of Fig. 11 shows that FCM_SICM can segment the background and the target, but there are some misclassified pixels in the boundary region between the black forest and the white snow and a few noise points in the black forest. The segmentation result of IFLICMLNLI is worse than FCM_SICM. None of the comparison algorithms except FCM_SICM and IFLICMLNLI can obtain ideal segmentation results. In the segmentation result of the proposed algorithm, the details of the wolf are well preserved, the number of misclassified pixels in the boundary region between the upper and lower backgrounds is reduced and the noise pixels in the background are well recovered. When mixed noise is added into Fig. 10(d), some clouds in the sky have closer gray value to the aircraft, resulting in all comparison algorithms cannot segment the aircraft contour effectively. Although the proposed algorithm classifies some clouds in the lower left corner and some noise pixels as aircraft, the aircraft contour is completely segmented, other clouds and noise points are accurately segmented as background. The segmentation numerical results are shown in Table 7. In summary, the proposed algorithm not only has better segmentation visual effect on the real image contaminated with noise, but also has better evaluation indexes than comparison algorithms and stronger robustness to noise.

4.5 Results on SAR images

In order to further test the segmentation performance of the proposed algorithm, six remote sensing SAR images from NWPU-RESISC45 dataset [35] are selected for experiments in this section. As shown in Fig. 12, which are #aircraft_086, #cloud_494, #circular_farmland_130, #golf_course_332, #island_401 and #lake_103. All images in Fig. 12 are corrupted by 10% mixed noise. The noisy images and their segmentation results are shown in Fig. 13.

It can be seen from Fig. 13 that most of the comparison algorithms cannot effectively segment the target in noisy SAR images and there are a large number of noise pixels and misclassified pixels in the segmentation results. FLICM only segments the cloud in Fig. 12(b) and FCM_SICM only segments the circular farmland in Fig. 12(c). IFLICMLNLI can segment part of the target's contour, but it incorrectly
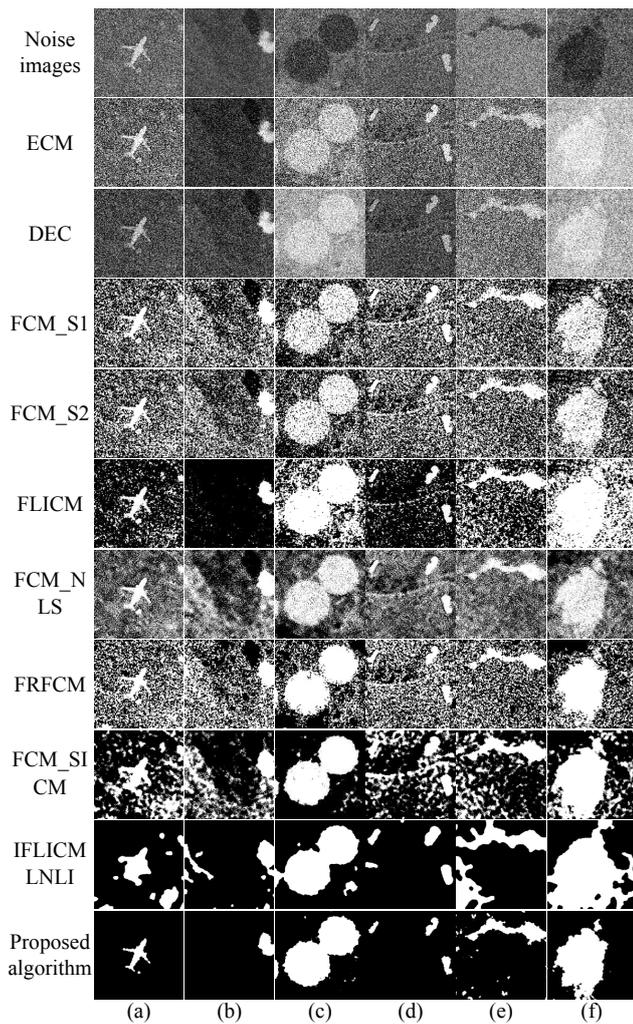
It can be seen from Fig. 11 that for the hill image shown in Fig. 10(a), due to the influence of mixed noise, there are a large number of misclassified pixels in boundary regions between different clusters in the segmentation results of comparison algorithms. The proposed algorithm segments the boundary regions between different clusters that are heavily contaminated by noise more accurately. Fig. 10(b) contains three clusters, all comparison algorithms segment the birds and the sky into the same cluster, while the noise-contaminated branch background is segmented into two clusters. The proposed algorithm segments the three clusters contained in the image more accurately and a large number of noise pixels are suppressed, although there are a small number of misclassified pixels in bird's edge and branch background. Figs. 10(c) and (d) contain three clusters. The moon in Fig 10(c) and the wolf in Fig 10(d) has fewer pixels. It can be seen from the third column of Fig. 11 that only the proposed algorithm obtains the segmentation result close

Fig. 13 Segmentation results on SAR images with 10% mixed noise, **a** #airplane_086, **b** #cloud_494, **c** #circular_farmland_130 , **d** #golf_course_332, **e** #island_401 and **f** #lake_103
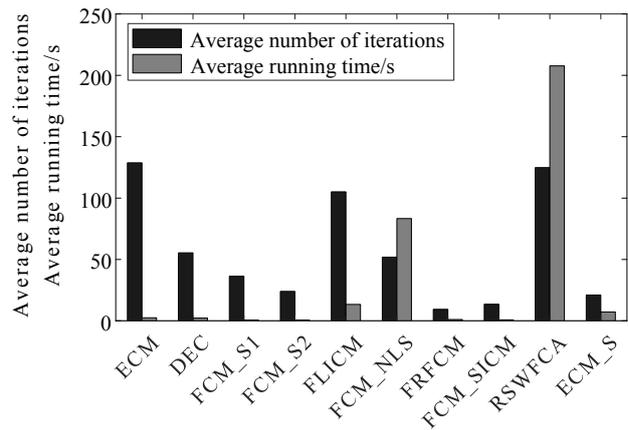

Fig. 14 Average number of iterations and average running time of ten algorithms

4.6 Number of iterations and running time

The number of iterations and running time are common indexes to estimate the efficiency of clustering algorithm. All the experimental images in sections 4.3, 4.4 and 4.5 are selected. As shown in Fig. 14, the average number of iterations and average running time of all algorithms are counted, which are presented in the form of histogram.

It can be seen from Fig. 14 that the average number of iterations of the proposed algorithm is relatively less, because this algorithm assigns noise pixels to the noise cluster, reducing the impact of noise pixels on the iteration. But the proposed algorithm is higher than FRFCM and FCM_SICM on the whole. Because FRFCM is a histogram-based clustering algorithm, FCM_SICM reduces the number of iterations by introducing membership linking in the objective function.

It is also clear from Fig. 14 that the average running time of FCM_NLS, IFLICMLNLI and the proposed algorithm is significantly higher than other comparison algorithms. Due to the large search window of FCM_NLS, the non-local mean filtering consumes a lot of time. IFLICMLNLI has slow convergence and many iterations, resulting in the longest average running time. Compared with the above two algorithms based on non-local information, the proposed algorithm improves the execution efficiency and the average running time is shorter.

In summary, although the average number of iterations of the proposed algorithm is relatively less, the recovery of noise pixels consumes more running time.

5 Conclusion

This paper mainly studies the gray image segmentation based on evidence clustering and proposes a robust evidence c-

classifies the heavily noise-contaminated region in the background as the target. At the same time, there is a serious misclassification on the edge of the object and the image details cannot be preserved, resulting in a large difference between the segmentation result and the original image. The proposed algorithm not only accurately segments the target in the image, but also retains more detailed information and the noise pixels are better suppressed.

Since there is no ground truth, the clustering validity evaluation indexes V_{pc} and V_{pe} as well as the image quality evaluation index PSNR are used to evaluate the segmentation results. The segmentation numerical results are shown in Table 8. It can be seen that V_{pc}, V_{pe} and PSNR of the proposed algorithm are better than all comparison algorithms.

In summary, the proposed algorithm has stronger noise suppression ability and better detail retention ability, which can achieve effective segmentation for noisy SAR images.

Table 8 Quantization results of ten algorithms on SAR images

Image	Index	ECM	DEC	FCM_S1	FCM_S2	FLICM	FCM_NLS	FRFCM	FCM_SICM	IFLICM_LNLI	Proposed
Fig.13(a)	V_{pc}	0.7391	0.7602	0.5559	0.6350	0.6248	0.5364	0.6935	0.6298	0.7638	**0.9801**
	V_{pe}	0.1744	0.1637	0.2748	0.2347	0.2416	0.2839	0.2043	0.2393	0.1723	**0.0175**
	PSNR	9.1565	10.5021	15.2900	19.6571	18.7333	19.8197	18.3368	20.2901	20.5029	**23.9212**
Fig.13(b)	V_{pc}	0.7372	0.7599	0.5937	0.4952	0.7681	0.5001	0.6660	0.6458	0.8031	**0.9883**
	V_{pe}	0.1747	0.1629	0.2563	0.3709	0.1653	0.3010	0.2200	0.2304	0.1492	**0.0113**
	PSNR	7.9263	8.9280	12.1381	18.3774	13.8949	17.2680	13.0294	17.9943	12.7836	**22.0637**
Fig.13(c)	V_{pc}	0.7605	0.7846	0.6160	0.6857	0.6454	0.6285	0.6607	0.7693	0.7976	**0.9400**
	V_{pe}	0.1598	0.1480	0.2455	0.2089	0.2307	0.2391	0.2228	0.1668	0.1525	**0.0461**
	PSNR	9.8523	10.4535	18.5733	19.4052	18.2534	18.9290	20.1967	21.2924	20.5807	**24.0634**
Fig.13(d)	V_{pc}	0.7470	0.7711	0.5564	0.6390	0.6478	0.5331	0.6963	0.6264	0.7716	**0.9797**
	V_{pe}	0.1685	0.1564	0.2745	0.2326	0.2298	0.2854	0.2028	0.2408	0.1682	**0.0181**
	PSNR	9.5041	10.5057	19.6530	19.7471	19.5961	19.6974	18.4948	20.0480	20.3614	**24.4691**
Fig.13(e)	V_{pc}	0.7301	0.7450	0.5496	0.6268	0.5861	0.5323	0.7071	0.6180	0.7549	**0.9280**
	V_{pe}	0.1801	0.1726	0.2777	0.2388	0.2608	0.2858	0.1969	0.2450	0.1770	**0.0541**
	PSNR	7.7999	9.7325	14.4756	14.1074	18.8839	14.3844	13.3886	14.1619	24.0280	**26.3948**
Fig.13(f)	V_{pc}	0.7723	0.7953	0.5962	0.6804	0.6541	0.5878	0.6713	0.7262	0.7693	**0.9324**
	V_{pe}	0.1517	0.1407	0.2552	0.2116	0.2262	0.2592	0.2171	0.1876	0.1684	**0.0517**
	PSNR	9.7361	10.4752	18.1703	19.5426	17.6150	18.5274	19.6118	18.8595	18.6848	**24.1004**

means clustering combining spatial information for image segmentation algorithm, then applies it to the segmentation of noisy image. In order to improve the capability of ECM to detect noise points, this paper first calculate the probability that the pixel is a noise point utilizing the local information of pixels, and then construct an adaptive noise distance utilizing the noise probability and assign noise points to the noise cluster according to the adaptive noise distance, thus the adverse effect of noise on updating the cluster center is overcome.Next, the original information, local information and non-local information of pixels are introduced into the distance metric through adaptive weight, which further improves the robustness of the proposed algorithm while preserving rich image details. In the iteration, the entropy of pixel membership degree is used to design an adaptive parameter to solve the problem of selecting the distance parameter in CCM. Through the iterative formula, a credal partition is derived. Because there are pixels belonging to the meta-cluster and the noise cluster in the credal partition, the Dempster's rule of combination was improved by introducing spatial neighborhood information. Using this combination rule, the meta-clusters are first specified, and then the noise cluster is recovered to obtain a complete segmentation image. In order to verify the effectiveness of the proposed algorithm, synthetic images, real images and SAR images are used for experiments. The experimental results show that the proposed algorithm has better noise suppression ability and detail retention ability for experimental images contaminated by mixed noise, and its segmentation performance and clustering performance are better than the related comparison algorithms. The segmentation model of the proposed algorithm makes full use of local information, non-local information and noise distance. However, it takes long time to specify meta-clusters and recover the noise cluster. There-

fore, how to shorten the running time of the proposed algorithm and design an efficient noise cluster recovery strategy to improve the practicability will be the next research goal.

Statements and Declarations

References

1. Kukreja V (2023) Image Segmentation Techniques: Statistical, Comprehensive, Semi-Automated Analysis and an Application Perspective Analysis of Mathematical Expressions. ARCH COMPUT METHOD E 30(1):457-495 https://doi.org/10.1007/s11831-022-09805-9

2. Abualigah L, Al-Okbi N K, Elaziz M A et al (2022) Boosting marine predators algorithm by salp swarm algorithm for multilevel thresholding image segmentation. MULTIMED TOOLS APPL 81(12):16707-16742 https://doi.org/10.1007/s11042-022-12001-3

3. Shang R, Liu M, Jiao L et al (2022) Region-level SAR image segmentation based on edge feature and label assistance. IEEE T GEOSCI REMOTE 60:1-16 https://doi.org/10.1109/TGRS.2022.3217053

4. Fang J, Liu H, Liu J et al (2021) Fuzzy region-based active contour driven by global and local fitting energy for image segmentation. Appl Soft Comput 100:106982 https://doi.org/10.1016/j.asoc.2020.106982

5. Devi M A, Sheeba J I, Joseph K S (2022) Neutrosophic graph cut-based segmentation scheme for efficient cervical cancer detection. J KING SAUD UNIV-COM 34(1):1352-1360 https://doi.org/10.1016/j.jksuci.2018.09.014

6. Hooda H, Verma O P (2022) Fuzzy clustering using gravitational search algorithm for brain image segmentation. MULTIMED TOOLS APPL 81(20):29633-29652 https://doi.org/10.1007/s11042-022-12336-x

7. Ezugwu A E, Shukla A K, Agbaje M B et al (2021) Automatic clustering algorithms: a systematic review and bibliometric analysis of relevant literature. Neural Comput Appl 33(11):6247-6306 https://doi.org/10.1007/s00521-020-05395-4

8. Mittal H, Pandey A C, Saraswat M et al (2021) A comprehensive survey of image segmentation: clustering methods, performance parameters, and benchmark datasets. Multimed Tools Appl 81(24): 35001-35026 https://doi.org/10.1007/s11042-021-10594-9

9. Miyamoto S, Ichihashi H, Honda K et al (2008) Algorithms for fuzzy clustering. Springer, Heidelberg

10. Dave R N (1991) Characterization and detection of noise in clustering. Pattern Recogn Lett 12(11):657-664 https://doi.org/10.1016/0167-8655(91)90002-4

11. Ahmed M N, Yamany S M, Mohamed N et al (2002) A modified fuzzy c-means algorithm for bias field estimation and segmentation of MRI data. IEEE T Med Imaging 21(3):193-199 https://doi.org/10.1109/42.996338

12. Chen S, Zhang D (2004) Robust image segmentation using FCM with spatial constraints based on new kernel-induced distance measure. IEEE Trans Syst Man Cybern B 34(4):1907-1916 https://doi.org/10.1109/TSMCB.2004.831165

13. Zhao F, Jiao L, Liu H (2011) Fuzzy c-means clustering with non local spatial information for noisy image segmentation. Front Comput Sci Chi 5(1):45-56 https://doi.org/10.1007/s11704-010-0393-8

14. Krinidis S, Chatzis V (2010) A robust fuzzy local information C-means clustering algorithm. IEEE T Image Process 19(5):1328-1337 https://doi.org/10.1109/TIP.2010.2040763

15. Lei T, Jia X, Zhang Y et al (2018) Significantly fast and robust fuzzy c-means clustering algorithm based on morphological reconstruction and membership filtering. IEEE T Fuzzy Syst 26(5):3027-3041 https://doi.org/10.1109/TFUZZ.2018.2796074

16. Wang Q, Wang X, Fang C et al (2020) Robust fuzzy c-means clustering algorithm with adaptive spatial & intensity constraint and membership linking for noise image segmentation. Appl Soft Comput 92:106318 https://doi.org/10.1016/j.asoc.2020.106318

17. Zhang X, Sun Y, Liu H et al (2021) Improved clustering algorithms for image segmentation based on non-local information and back projection. Inform Sciences 550:129-144 https://doi.org/10.1016/j.ins.2020.10.039

18. Song Q, Wu C, Tian X et al (2022) A novel self-learning weighted fuzzy local information clustering algorithm integrating local and non-local spatial information for noise image segmentation. Appl Intell 52(6):6376-6397 https://doi.org/10.1007/s10489-021-02722-7

19. Masson M H, Denoeux T (2008) ECM: An evidential version of the fuzzy c-means algorithm. Pattern Recogn 41(4):1384-1397 https://doi.org/10.1016/j.patcog.2007.08.014

20. Liu Z G, Dezert J, Mercier G et al (2012) Belief c-means: An extension of fuzzy c-means algorithm in belief functions framework. Pattern Recogn Lett 33(3):291-300 https://doi.org/10.1016/j.patrec.2011.10.011

21. Liu Z G, Pan Q, Dezert J et al (2015) Credal c-means clustering method based on belief functions. Knowl-Based Syst 74(1):119-132 https://doi.org/10.1016/j.knosys.2014.11.013

22. Su Z, Zhou H, Wang P et al (2018) E2CM: An evolutionary version of evidential C-means clustering algorithm. In: Belief Functions: Theory and Applications: 5th International Conference, BELIEF 2018, pp 234-242 https://www.doi.org/10.1007/978-3-319-99383-6_29

23. Zhang Z W, Liu Z, Martin A et al (2021) Dynamic evidential clustering algorithm. Knowl-Based Syst 213(4):106643 https://doi.org/10.1016/j.knosys.2020.106643

24. Zhu Y M, Bentabet L, Dupuis O et al (2002) Automatic determination of mass functions in Dempster-Shafer theory using fuzzy c-means and spatial neighborhood information for image segmentation. Opt Eng 41(4):760-770 https://doi.org/10.1117/1.1457458

25. Wen J, Yang T, Shou Y et al (2018) Improved evidential fuzzy c-means method. J Syst Eng Electron 29(1):187-195 https://doi.org/10.21629/JSEE.2018.01.19

26. Makni N, Betrouni N, Colot O (2014) Introducing spatial neighbourhood in Evidential C-Means for segmentation of multi-source images: Application to prostate multi-parametric MRI. Inform Fusion 19:61-72 https://doi.org/10.1016/j.inffus.2012.04.002

27. Wang F, Lian C, Vera P et al (2019) Adaptive kernelized evidential clustering for automatic 3D tumor segmentation in FDG-PET images. Multimedia Syst 25(2):127-133 https://doi.org/10.1007/s00530-017-0579-0

28. Shafer G (1976) A mathematical theory of evidence. Taylor & Francis Group, Oxford

29. Smets P (2005) Decision making in the TBM: the necessity of the pignistic transformation. Int J Approx Reason 38(2):133-147 https://doi.org/10.1016/j.ijar.2004.05.003

30. Mendonca A M, Campilho A (2006) Segmentation of retinal blood vessels by combining the detection of centerlines and morphological reconstruction. IEEE T Med Imaging 25(9):1200-1213 https://doi.org/10.1109/TMI.2006.879955

31. Alpert S, Galun M, Brandt A et al (2011) Image segmentation by probabilistic bottom-up aggregation and cue integration. IEEE T Pattern Anal 34(2): 315-327 https://doi.org/10.1109/TPAMI.2011.130

32. Arbelaez P, Maire M, Fowlkes C et al (2010) Contour detection and hierarchical image segmentation. IEEE T Pattern Anal 33(5):898-916 https://doi.org/10.1109/TPAMI.2010.161

33. Cheng G, Han J, Lu X (2017) Remote sensing image scene classification: Benchmark and state of the art. P IEEE 105(10):1865-1883 https://doi.org/10.1109/JPROC.2017.2675998

34. Covoes T F, Hruschka E R, Ghosh J (2013) A study of k-means-based algorithms for constrained clustering. Intell Data Anal 17(3):485-505 https://doi.org/10.3233/IDA-130590

35. Girshick R, Donahue J, Darrell T et al (2014) Rich feature hierarchies for accurate object detection and semantic segmentation. In: Proceedings of the IEEE conference

on computer vision and pattern recognition, pp 580-587 https://doi.org/10.1109/CVPR.2014.81

36. Mukhopadhyay A, Maulik U (2011) A multiobjective approach to MR brain image segmentation. Appl Soft Comput 11(1):872-880 https://doi.org/10.1016/j.asoc.2010.01.007

37. Guo Y, Sengur A (2013) A novel color image segmentation approach based on neutrosophic set and modified fuzzy c-means. Circ Syst Signal Pr 32(4):1699-1723 https://doi.org/10.1007/s00034-012-9531-x

38. Bezdek J C (1973) Cluster validity with fuzzy sets. Journal of Cybernetics 3(3):58-73 https://doi.org/10.1080/01969727308546047

39. Bezdek J C (1975) Mathematical models for systematics and taxonomy. In: Proceedings of 8th International Conference on Numerical Taxonomy, pp 143-166